In-Situ Ultrasonic Monitoring for Viscoelastic Properties of Being-printed Part during Digital Light Processing based Photopolymer Additive Manufacturing

by

Tong Su

Bachelor of Science, University of Pittsburgh, 2019

Submitted to the Graduate Faculty of the

Swanson School of Engineering in partial fulfillment

of the requirements for the degree of

Master of Science in Mechanical Engineering

University of Pittsburgh

2021

UNIVERSITY OF PITTSBURGH

SWANSON SCHOOL OF ENGINEERING

This thesis was presented

by

Tong Su

It was defended on

April 6, 2021

and approved by

Xiayun Zhao, PhD, Assistant Professor, Department of Mechanical Engineering and Material Science

Qing-Ming Wang, PhD, Professor, Department of Mechanical Engineering and Material Science

Tevis Jacobs, PhD, Associate Professor, Department of Mechanical Engineering and Material Science

Thesis Advisor: Professor. Xiayun Zhao, PhD, Department of Mechanical Engineering

In-Situ Ultrasonic Monitoring for Viscoelastic Properties of Being-printed Part during Digital Light Processing based Photopolymer Additive Manufacturing

Tong Su, M.S

University of Pittsburgh, 2021

Photopolymer additive manufacturing (PAM) processes such as Stereolithography (SLA) and Digital Light Processing (DLP) employ photopolymerization reactions to crosslink monomers layer by layer under light exposure schemes corresponding to the cross-sections of a target object. Such processes have been widely used in various applications, from rapid prototyping to biomedical implants, soft robotics, and flexible electronics. In-situ process monitoring is critical for process optimization and control to achieve precise structures and desired properties via PAM. As existing research focuses on the online measurement of part geometry, there lack in-situ monitoring technologies to obtain real-time information about the material properties of PAM printed parts, especially the viscoelastic properties that will affect the stress-strain and deformation behaviors of curing and cured parts. This work develops the first-ever in-situ ultrasonic measurement (IUM) method, cost-effective and non-destructive, for DLP process monitoring. Experimental study is performed for monitoring a variety of process conditions (i.e., exposure time, intensity, layer thickness, and build stage speed) to exemplify that the developed IUM method based on ultrasonic longitudinal wave sensing can probe the evolving Young's modulus, viscoelastic damping ratio, and loss factor of a being-printed part. Standard measurement and nanoindentation testing results are obtained offline to validate the IUM results. This novel IUM method will offer unique insights into process-property relationships for PAM processes modeling and real-time feedback control, facilitating 3D and 4D printing of sophisticated products such as soft robots that require localized manipulation of mechanical properties.

Table of Contents

List of Tables

List of Figures

Acknowledgement

Firstly, I want to thank my advisor, Dr. Xiayun Zhao. Her acumen in the field of research practice provides strong guidance during my Master thesis research. Her passion for academics stimulates me to fulfill my goal regards to my research practice.

Secondly, I want to thank my lab mate, Dr. Chaitanya Vallabh, who sets a good role model. He helped me tremendously in the past two years with his solid knowledge, kind personality, and research passion.

Thirdly, I want to thank my committee member for their interests and supports in my thesis. Also, I want to thank my labmate, Mr. Yubo Xiong, for his generous help to improve my skill in programming and data analysis, as well as my research partner Ms. Yue Zhang for her good collaborations during our experiments.

Most importantly, I want to thank my family for their understanding and support during all these years when I studied at the University of Pittsburgh.

1.0 Introduction

1.1 Additive Manufacturing with Digital Light Processing

Additive manufacturing (AM) is a prominent advanced manufacturing technology, well known as 3D printing, and has been widely used in rapid prototyping and various industries such as aerospace and biomedicine (Ian Gibson 2015). It has the potential to break constraints of the traditional manufacturing process, such as material wastage, time consumption, and geometry limitation. Typical AM processes include Fused Deposition Modeling (FDM), Digital Light Processing (DLP), and Laser Power Bed Fusion (LPBF).

DLP is a photopolymerization-based AM (PAM) process that uses a digital light projector to deliver a patterned light beam that will selectively cure a liquid photosensitive resin layer by layer process Illustration for a typical DLP system is shown in Figure 1.

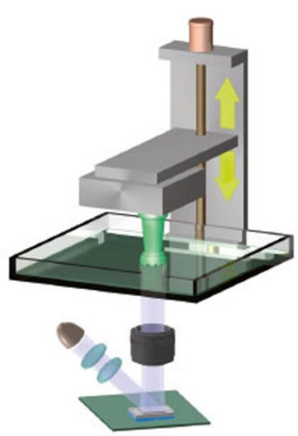

Figure 1: Schematic for a typical DLP machine(Tang 2005)

A basic DLP printing process goes with the following steps:

1: A 3-D model created in a CAD program.

2: Slices the 3-D model into series of thin horizontal layers.

3. Sliced 3-D model profiles were used as layer curing patterns and transferred to the laser system that scans the bottom layer of the photosensitive resin, curing it.

4. The newly built layer will be attached to the building platform, then the platform is raised to a one-layer distance above the bottom of the resin chamber. This process repeats layer by layer, with successive layer to layer bonding, until the part is completed.

The properties of DLP printed parts are greatly affected by the printing process conditions. The key printing process parameters that can be adjusted to achieve optimal printing quality include curing layer exposure time, layer thickness, and build head moving speed. These factors critically determine the mechanical properties of a DLP printed part (Hornbeck 1996).

1.2 Photopolymerization Kinetics in DLP Process

There are two basic types of polymerization: step polymerization and chain polymerization. In step polymerization, the chemical reaction proceeds by combining functional groups between two reactants with a slow reaction speed. In chain polymerization, it is required to have a catalyst to initiate the chemical reaction.(Odian 2004) Due to the generation of free radicals, the free radical chain polymerization can be activated by light, voltage, chemical redox, or mechanical. In a PAM process, the chain polymerization process uses light to trigger photo initiators and generate free radicals(Chen, Zhong et al. 2016) Such light-induced polymerization has many advantages, including a high reaction rate and broad material choice. Most importantly, it has a rapid polymer chain formation rate; which verified that photopolymers are the most consumed 3D printing materials (Kuar 2002) (Wohlers 2016).

A photopolymerization process typically includes four steps: photo-decomposition, initiation, propagation, and termination(Andrejewska 2001).

The chemical kinetics follows these steps(Wu 2018):

$$\text{Photodecomposition: } \mathrm{P} \rightarrow 2\mathrm{R}^{*}$$

$$\text{Initiation: } \mathrm{R}^{*} + \mathrm{M} \rightarrow \mathrm{RM}^{*}(\mathrm{P}^{*})$$

$$\text{Propagation: } \mathrm{P}^{*} + \mathrm{M} \rightarrow \mathrm{P}^{*}$$

$$\text{Termination:} \mathrm{P}^{*} + \mathrm{P}^{*} \rightarrow \mathrm{P}_{\mathrm{dead}}$$

During the initiation process photo initiator will be triggered by ultraviolet (UV) or visible light with an electron or photo donor to produce free radical. These free radicals will be paired with oligomer and monomers from polymer chains during the propagation process. Then, the polymer chains are condensed into a polymer network and terminated when radicals are consumed. With the rapid liquid to solid phase transition the molecular wight, polymer chain length, and crosslink density evolves (Jiang 2018).

In a PAM process such as DLP, the degree of conversion (or degree of crosslinking, DoC) of the monomers/oligomers or the functional groups is mainly determined by light intensity and exposure time. DoC is a primary metric for PAM performance as many material properties such as density and elastic modulus can be evaluated in terms of DoC (2018, Jiang 2018). In polymer science, DoC is a good indication of average composition of a polymerized material system and can be more easily measured than the polydispersity index. Thus, DoC is used to characterize and model material properties in traditional curing of thermosetting coating and adhesives as well as in PAM. In this study, we will adopt Fourier transform infrared spectroscopy (FTIR) to measure

DoC of printed parts and calculate the elastic modulus using a literature model that is a function of DoC.

1.3 In-situ Monitoring for Photopolymer Additive Manufacturing

Various metrology and measurement methods have been adapted to characterize and test the properties of additively manufactured parts in situ. One of the mostly used methods is using camera and imaging techniques to visualize geometry and detect defects of a printed part.

Despite active research on in-situ monitoring for metal-based AM, there are only a few literatures reported on PAM process monitoring (Zhao, X., Rosen, D,W., 2017) developed an in-situ interferometric curing monitoring and measurement (ICM) system for a custom PAM setup that features static stage and is different from general DLP processes.The ICM approach is demonstrated to be able to measure the thickness profile of cured part in real time and can be used to control 3D geometry. (Zhao, X., Rosen, D.W., 2018) Yet, this ICM method cannot provide information on material properties. Higgins et al. integrated an atomic force microscopy (AFM) with a DLP system is used to probe a just-printed voxel's modulus, measure the cure depth, and sense the liquid resin's rheology (Higgins 2020). However, the detector tip needs to be emersed into the part and liquid resin, causing liquid perturbation and detrimental effects on part formation. Therefore, this AFM method is expensive, intrusive, limited for research machines only, and cannot be implemented on commercial DLP systems.

To conclude, in-situ non-destructive monitoring technology is much desired to measure the properties of printed material during PAM. Common non-destructive testing (NDT) methods used for AM include acoustic emission and ultrasonic testing(C.H.Wong 2017). The instrumentation system for such soundwave-based testing methods consists of signal acquisition and diagnosis, processing, and analysis units. Is used to identify the position of possible cracks during the printing process. Researchers have also used a compact ultrasonic sensor pair that consists of a signal transmitter and a signal receiver, which can be more compatible with AM machines. The in-situ ultrasonic sensor has been used to monitor defects and understand the defect generation and propagation in laser powder bed fusion (LPBF) metal AM (Venkata Karthik Nadipalli, 2018). The study also states that elastic modulus can be obtained for metals using ultrasonic measurement. Researchers develop a curve piezoelectric transducer and utilize longitudinal wave and Rayleigh wave to characterize Young's modulus of LPBF printed metal tensile bars(Li 2016). Another research group employed in-situ and ex-situ ultrasonic methods to study the real-time Young's modulus behavior during the fused deposition modeling (FDM) process(Xu 2017). However, none of these in-situ NDT methods have been applied to monitoring PAM processes.

1.4 Motivations and Objectives

Nonlinear viscoelastic properties are the main mechanical characteristics of polymeric materials and thus an important PAM research aspect for understanding the material property changes and structural deformation during photopolymerization process. (Charlesby 1992) Current studies rely on approaches of modeling and simulation to understand the non-equilibrium behaviors and material property evolution (Xiang, 2020)To the best of our knowledge, few literatures are available in-situ NDE techniques for monitoring dynamic properties of curing and cured material during PAM such as in-situ AFM monitoring to evaluate the sample stiffness and possible cracks in the printed part.

To fill the research gap of lacking an in-process non-destructive technology for monitoring viscoelasticity during PAM, the objective of this study is to develop an in-situ ultrasonic measurement (IUM) method based on the longitudinal wave travel principle to characterize the dynamically changing Young's Modulus and the damping ratio for curing and cured part during a DLP process. Data analytics methods are developed to process and interpret the IUM data. The developed IUM method is implemented to monitor and understand the DLP process-property relationships under a variety of process settings – i.e., different exposure time, exposure intensity, layer thickness, and build stage moving speed.

2.0 Development of a Novel in-situ Ultrasonic Measurement (IUM) System and Method for PAM Process Monitoring

In this chapter, a novel in-situ Ultrasonic Measurement (IUM) system is designed and the sensing data analytics method is developed to measure in process the being-printed part's viscoelastic properties.

2.1 IUM based on Ultrasonic Longitudinal Wave

As mentioned in section 1.3, in-situ ultrasonic measurement IUM has been adapted in LBPF and FDM additive manufacturing processes, but it has not been used in PAM process. To better understand the relation between the change in chemical reactions such as conversion of C=C bond to C-C bond (Degree of Curing) and the evolution of mechanical properties (such as Young's modulus) during the printing process.

Since the PAM process follows a layer-by-layer printing process, IUM method can be applied to find the real time Young's modulus during the printing process. To monitor the Young's modulus for the printed part after each layer has printed, this study applies in-situ ultrasonic measurement IUM method with one sensor works as signal source and signal receiver at a fixed location to send and receive ultrasonic wave signal to a printed part. This method could help us to find the corresponding longitudinal wave velocity after one layer has printed, which is later used in the calculate the Young's modulus in order to study its evolution during the printing process Our IUM system utilize longitudinal wave propagation in a 3D printed polymer part, once longitudinal wave propagates in our polymer part, it generates a displacement of a 3D printed polymer part. This displacement is always in the same direction of, or opposite direction to the wave propagation direction. Longitudinal wave propagates in a polymer part relates to its material and geometric quality

Since we use one sensor work to send and receive ultrasonic signal, we need to characterize the minimal detectable thickness for our excited ultrasonic signal. In this study we choose a piezoelectric ultrasonic sensor (NDT1-022K, TE connectivity, Schaffhausen, Switzerland) with a nominal central frequency of 3 MHz). To find the minimal detectable thickness of a 3MHz ultrasonic wave, we evaluate the corresponding wavelength (λ) is 205.6 μm with longitudinal wave velocity at 617 m/s. The minimal detectable thickness should be larger than 1.5* λ to allow ultrasonic signal to travels through the material and reflect back to the signal receiver, for our IUM system the minimal detectable thickness is 308.4 μm As shown in Figure 2(a) and (b) our IUM system doesn't show a much difference in the received signal at the first 6 layer of the printing process.

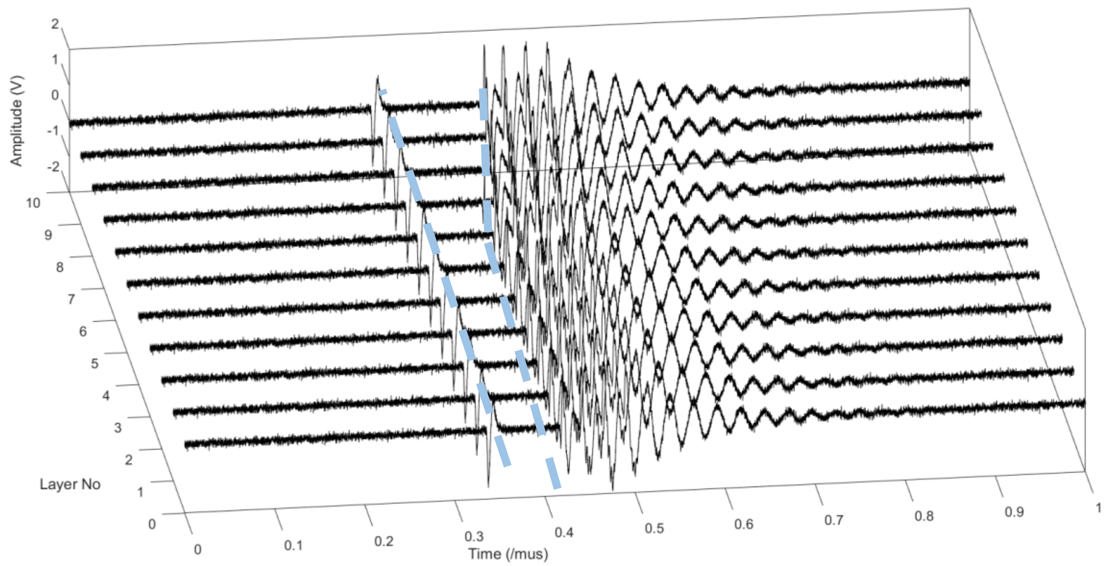

Figure 2: (a) Recieved First 10 Layer Signal from Set 1 Sample 1.3

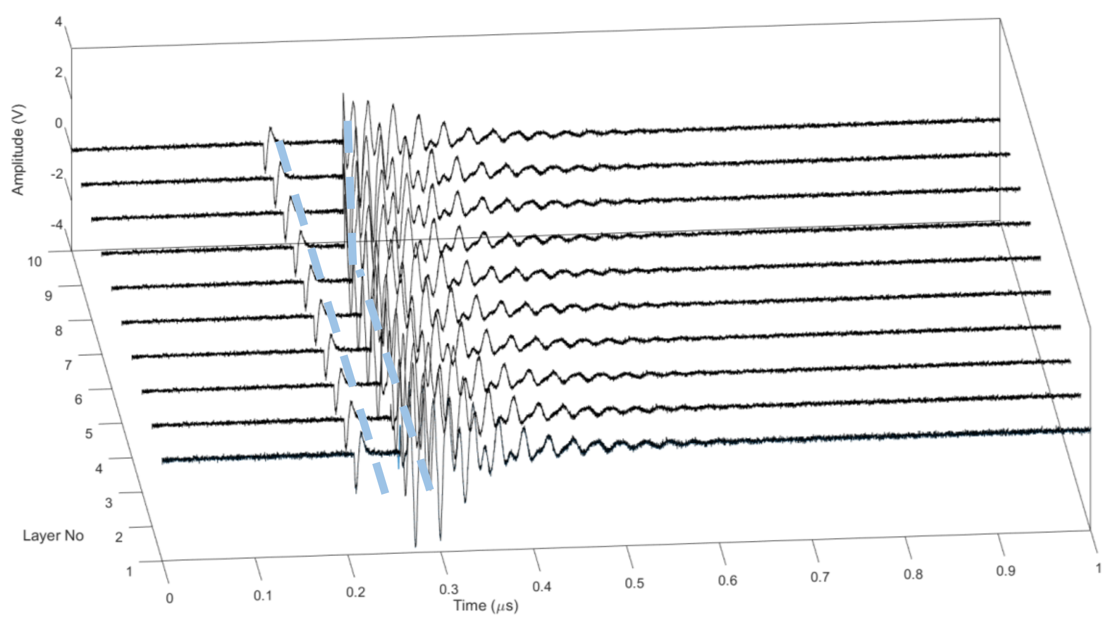

Figure 2(b): Recived First 10 Layer Signal From Set 2 Sample 1.2

2.2 IUM System Design

To acquire real time wave signal during the printing process a LabVIEW based wave spectrum acquisition system is used to record the wave spectrum after each new layer printed a representative of received signal spectrum shown in Figure 4. We will then analyze the signal with MATLAB signal processing toolbox by applying a high pass filter to remove high frequency noise. Process flow chart shown in Figure 3.

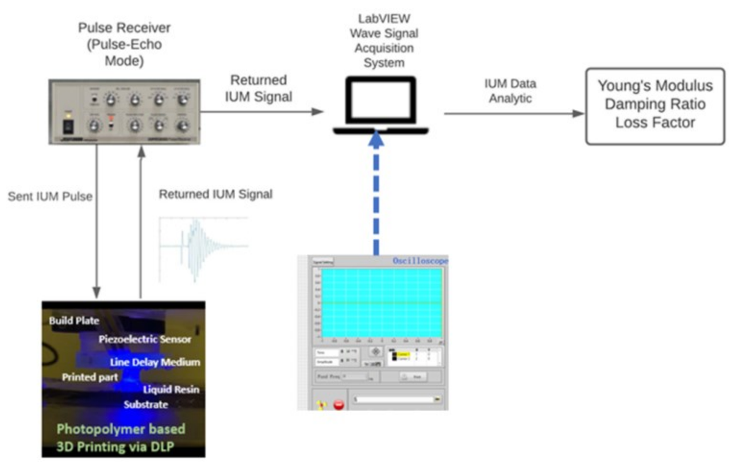

Figure 3: Process flow of the In-situ Ultrasonic Measurement System

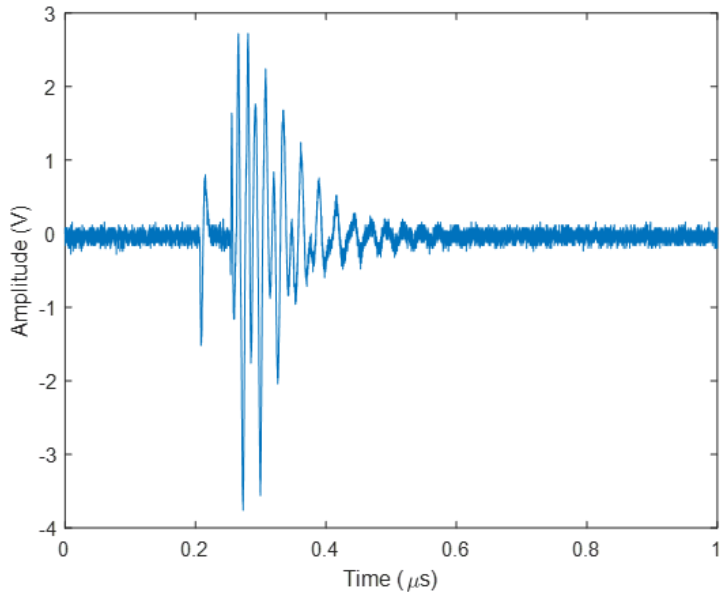

Figure 4: Representive Ultrasonic Signal Received by Sensor (Signal Corresponds to Sample 5, Layer 1)

The in-situ measurement setup is utilized to acquire the real-time pulse-echo (Krautkramer, J., Krautkramer, H., 2013)ultrasonic response from each print layer of a part for characterizing the properties of the as-printed part. During the experiment, the pulser receiver is set to excite the pulse at 3 MHz. with a pulse energy at 12.5 µJ, a default damping of 36 Ohms and default receiver signal gain at 0 operated with pulse echo mode. Ultrasonic pulse send from pulser receiver will excite the piezoelectric sensor which contact with elastomer delayed line material. Once printing process starts ultrasonic pulse will travel through the printed part until it reaches to the newly printed layer. Lastly a response signal obtained from printed part will reflects back to the sensor (Krautkramer, J., Krautkramer, H., 2013). The medium we use is a 0.7mm thick, elastomer delay line (Aqualene, Olympus, Waltham, MA), this delay line material also works as the built platform for the printed part during the experiments. IUM system set up shown in Figure 5.

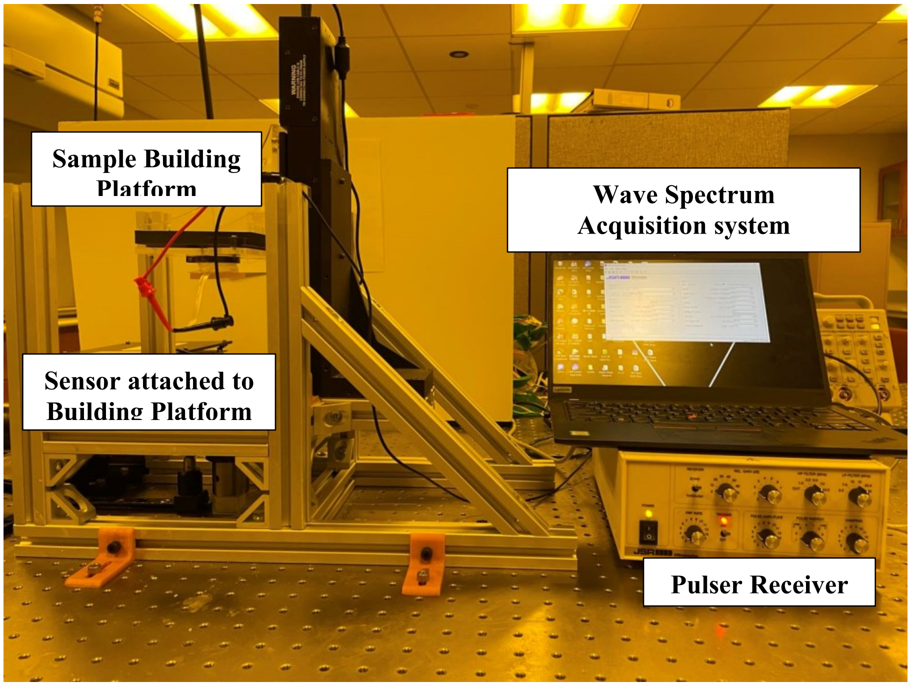

Figure 5: IUM System Componenets Set Up

2.3 Verifying the IUM Accuracy for Longitudinal Wave Velocity (C_l)

To validate the IUM accuracy for longitudinal wave velocity. Measured of Longitudinal wave velocity for AL1100 Aluminum (contains 99% of Aluminum) bar with dimension 10 cm*1.5cm* 0.65 mm at 4 different measurement locations. Where the Longitudinal wave velocity for aluminum is determined with measurement location thickness and time shift between reference signal and measurement's location signal with the following equation (Xu, X.,Vallabh, C.K.P., Cleland, Z. J., Cetinkaya, C., 2017):

$$C_l = h_s/\Delta_t \qquad 2\text{-}1$$

Where C_l is the longitudinal wave velocity, and Δ_t is the ToF (time of flight) corresponding to the printed layer corresponding C_l results shown in table 1 Compare to C_l provided by American Society for Testing and Material equals to 6420m/s the difference in Longitudinal wave velocity less than 6% where indicates a good measurement in C_l

Table 1: Value for Longitudinal wave in AL110 at Different Location and Corresponding Measurement Error Percentage

Measurement location	Cl (m/s) measured by IUM	Cl error%
1	6177	3.795%
2	6103	4.937%
3	6072	5.421%
4	6244	2.821%

2.4 IUM Data Analytics Method for measuring Young's Modulus

To discuss the evolution of Young's modulus during the printing process with, IUM in-situ measurements. We measured each printed part with its mass and volume, mass of the sample measured with weighing scale and volume of sample is calculated with cylinder lateral surface area and sample total thickness. The real-time Young's modulus of the material after each layer printed can be found using (Xu, X.,Vallabh, C.K.P., Cleland, Z. J., Cetinkaya, C., 2017):

$$E = \rho^2 * C_l \quad \text{2-2}$$

where ρ is the dynanmic printed part density, it is not a constant value due to different process setting. Sample density is high depends on the polymer chain corsslink, sample with more rigidly ordered polymer chain crosslink will give a higher value in sample density.

2.5 IUM Data Analytics Method for measuring Viscoelastic Damping Ratio and Loss Factor

To discuss the viscoelastic behavior of printed material, damping ratio and loss factor is discussed. Damping ratio represents the ultrasonic wave energy loss as it travels through the printed part, the damping ratio for each monitored wave signal is calculated using the logarithmic decrement method by choosing the consecutive decaying peaks in the received ultrasonic signal shown in figure 6 using the following equation:

$$\zeta = \frac{1}{\sqrt{1+\left(\frac{2\pi}{\delta}\right)^2}}, \delta = ln\frac{A_1}{A_2}\ , ln\frac{A_2}{A_3}\ , ln\frac{A_3}{A_4} \quad \text{2-3}$$

Where ζ is the calculated damping ratio, δ is the logarithmic decrement for two consecutive decaying peaks. The corresponding damping ratio for each decrement appears to be a constant. Based on the damping ratio we calculated the loss factor to evaluate the viscoelastic nature of polymer-based material using the following equation:

$$\tan(\delta) = 2 * \delta \qquad 2\text{-}4$$

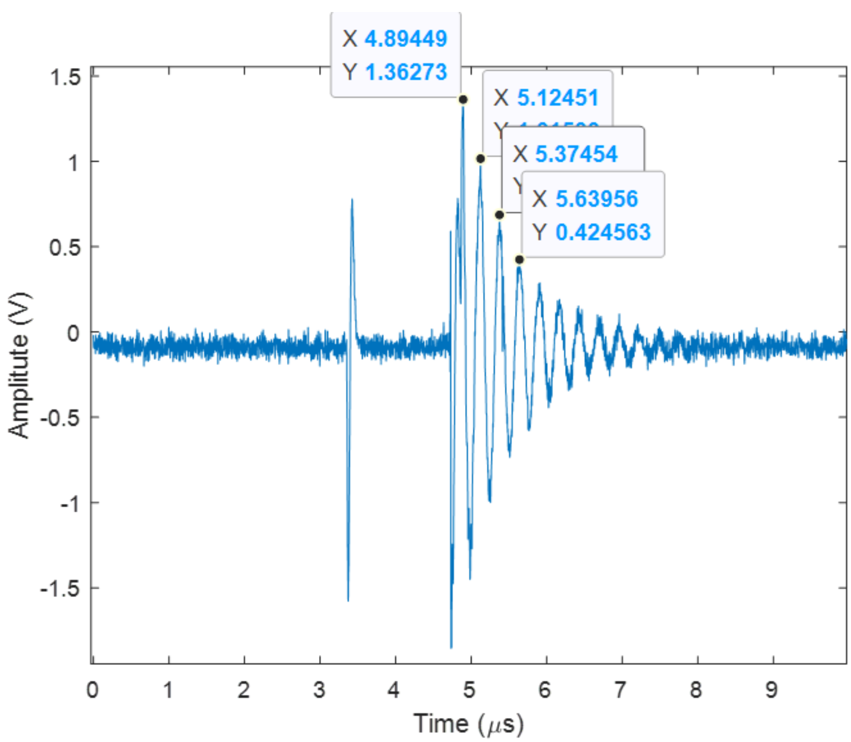

Figure 6: Consecutive Peaks in Signal Spectrum use to Evaluate Damping Ratio

3.0 Experimental Validation of IUM

This chapter presents the experimental validation of IUM with materials and methods. In this chapter, the PAM machine and materials utilized for the polymer resin preparation are discussed (Sections 3.1-3.2), followed by the experiment design (Section 3.2) and the ex-situ characterization and test methods section (Section 3.3).

3.1 Digital Light Processing based PAM Setup

Our Digital Light Processing (DLP) printer system shown in Figure 7, mainly consists of two digital micromirror devices (DMDs) (DLP 6500Pro Wintech Digital, Inc. CA) with principle operating wavelengths of 365 and 460nm respectively, a micro-linear stage (LTS 150, Thorlabs, NJ) and the required optical components for delivery and focusing of the printing pattern/image. The DMDs are controlled by custom written Python codes. Micro-linear stage is controlled using a custom written LabVIEW VI (NI Instrument Corporation, Austin, TX). The optical components used in the system are detailed in Table 3 and a optical schematic is shown in Figure 4. This system uses both bi-concave, bi-convex and a beam splitter to allow UV and blue light rays to reach the build plane.4. The beam splitter is used to split the Blue light beam and transmit it to the build plane. The bi-concave and bi-convex lenses are used for accurately propagating and focusing the print image on the build plane. All the optical components were purchased from Thorlabs (Table 3), unless specified.

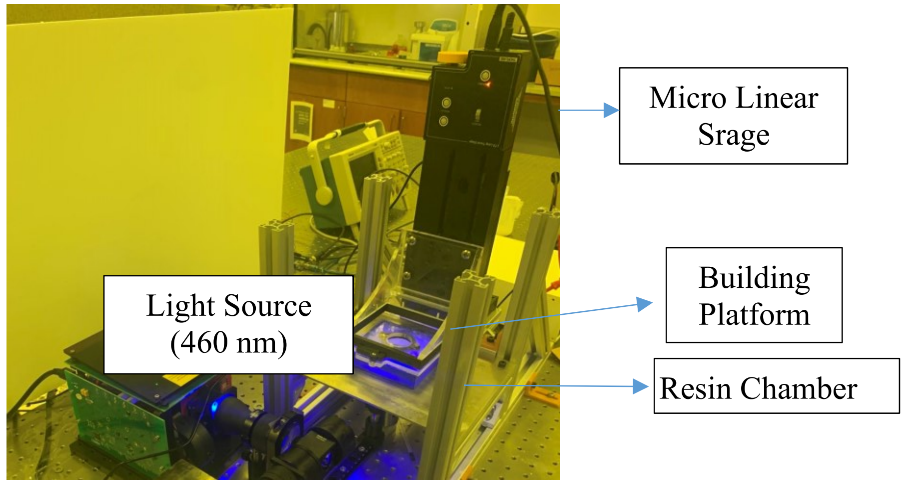

Figure 7: In-house DLP Printer Set Up

To understand the material behavior during the photo curing, it is also necessary to understand the actual light intensity reaching the build plane. The DLP process initiation reaction is controlled by the actual light density received for each printing layer. Light intensity *I* for each printing layer is expressed with the following equation(Tang 2005)

$$\mathrm{I} = \mathrm{I}_0 \exp\left\{-\frac{2 * t^2}{\mathrm{w}_0^2}\right\} * \exp(\mathrm{z}) \tag{3-1}$$

Where I_0 is the maximum intensity at the curing window, t is the exposure time for each layer, w_0 is the half radius of laser beam, z is the thickness of the curing part. In this study we control the output power intensity and projecting for the DMD system grayscale image are used, from the brightness at 255 to the darkest at 0. To investigate the changing of actual light intensity with different image shape, image size, and grayscale level. The light intensity I_0 (mW) at the curing window is measured with an optical power meter PM400 (Thorlabs, Inc, NJ, USA)

Theoretically, the relation between the image grayscale level (value) and the actual output intensity should be linear. To verify whether this is true in the real system, we project two set of circle images using eight different grayscales values from 0 to 255. For images with area smaller than the sensor area we use the image area to calculate the actual power intensity. For images larger than the sensor we use sensor area (0.785 cm^2) to calculate the actual intensity, measurements from different location are obtained.

The relation between actual power intensity for the same projecting image with different grayscale values are shown in Figure 8

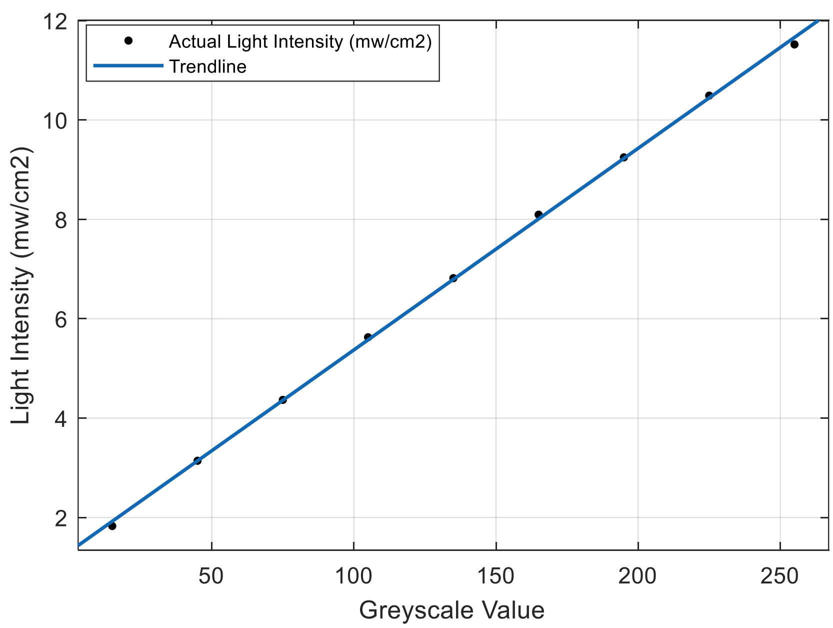

Figure 8 Relation between the grayscale and blue light intensity of a projected circle (area = 0.181 cm^2 at the build plane for curing all the samples. The relationship between these two parameters is linearly fitted R^2=0.9995.

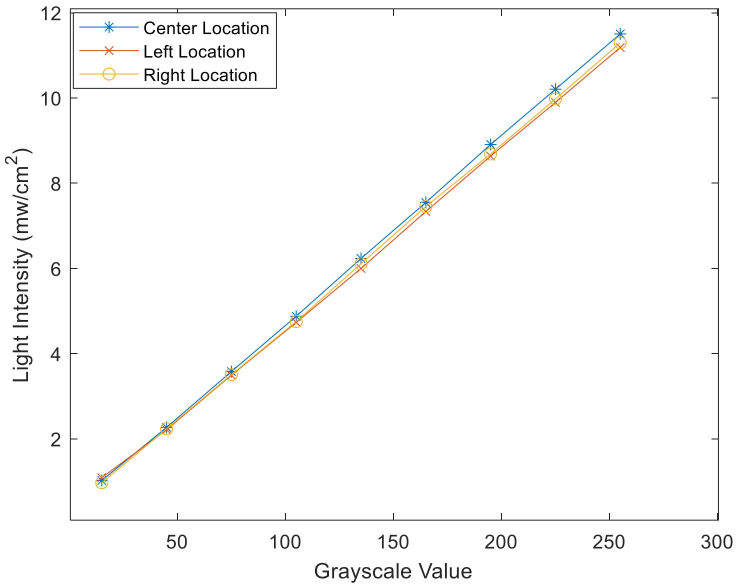

Figure 9: Relation between the grayscale level and blue light intensity with a projected circle (actual area=4.2748 cm2 at the build platform) at different measurement location. The relation between this two parameters is linear fitted at: R2=0.999

3.2 Materials Formulation and Preparation

In this study, Bisphenol A glycerolate dimethacrylate (Bis-GMA) and Triethylene glycol dimethacrylate (TEGDMA) were used as co-monomers for synthesizing the photopolymer resin. Camphorquinone (CQ) and Ethyl 4-dimethylaminobenzoate (EDAB) were used as co-photo-initiators. 2,2'-Bis(2-chlorophenyl)-4,4',5,5'-tetraphenyl-1,2'-biimidazole(o-Cl-HABI) (B1225, TCI America, Portland, OR, USA) was used as the UV photo-inhibitor. All the chemicals were acquired from Sigma-Aldrich (MO, USA) unless specified. All chemicals were used as received with no further modifications. The resin preparation along with the composition are detailed in the section 2.2.1.

In this study, the resin is prepared with an equal weight ratio composition of the monomers as detailed in Table1. The photo initiator and photo inhibitor ratio are chosen based on the resin curing behavior and the desired resin performance. This resin recipe was adapted from (Marting P de Beer, Harrt L, van der Laan, 2019). All the chemicals listed in Table 2 are added to a beaker and mixed using stirring magnetic equipment. The mixture is stirred for at least 3 hours to allow the proper dissolution of all the chemical components. All the resin preparation is performed in a light-sensitive environment to prevent undesired curing of the material. During the photopolymerization process, the liquid resin experiences a rapid liquid to solid phase transition in a few seconds. The prepared resin is then stored in amber bottles to prevent any photopolymerization.

Table 2: Weight Percentage for Each Chemical in Resin Preparation

Property of Chemical	Abbreviation of Chemical	Weight Percentage
Photo Initiator	CQ	0.2%
Photo Initiator	EDAB	0.5%
Monomer	TEGDMA	50%
Co-monomer	BisGMA	50%
Photo Inhibitor	HABI	3%

3.3 Design of Experiment

To understand the IUM characteristics and assess its capability of real-time PAM process monitoring, the experiment is designed as per the following considerations.

First, although IUM can measure a being-printed part's properties throughout the process - within each layer and between very two consecutive layers (i.e., at customizable measurement intervals), only the last measurement of the entire part that consist of all layers can be directly comparable with the offline post-build characterization results due to lack of standard scientific equipment for in-process characterization of PAM parts. Therefore, to demonstrate that IUM can measure during the PAM process a partially printed or intermediate part's property, two sets of experiment are designed with different number of layers. Thus, the samples of fewer layers will be used as mimics of intermediates for the samples of more layers, and ex-situ measurement results of the fewer-layer samples can be used to verify the IUM results for the more-layer samples' corresponding intermediate parts. Under the same process setting, one sample is printed in each of the two experimental sets, providing two groups of data for assessing the repeatability of IUM during the common number of layers. The two experimental sets together serve to evaluate the accuracy of IUM for being-printed and final-printed parts.

Moreover, a typical PAM process involves multiple key parameters that could affect the part's material properties. To evaluate whether the IUM method can discern the changes in part viscoelastic properties in response to potential changes in process dynamics, four key process parameters (build stage speed, layer exposure time, layer thickness, and layer exposure intensity) are varied, one at each group. Experiment with these groups of process settings will demonstrate the sensitivity of IUM as well as its utility for PAM process-structure relationship modeling and real-time feedback control.

Specifically, the experiment consists of two sets – Set 1 and Set 2, differentiated by the number of printed layers in each sample. Each sample has 200 layers in Set 1 and 10 layers in Set 2. Each set contains four groups that vary the build stage speed, layer exposure time, layer thickness, and exposure intensity, respectively. In each set, a total of 17 samples are printed under the varying printing conditions as listed in Table 2.

The targeted size of each cylindrical sample is: diameter = 8mm (area = 0.5024 cm^2) and a cured part thickness =1cm for Set 1 group 1,2,4 samples, cured part thickness=0.5cm for Set 1 sample 3.1, cured part thickness=1.3 cm for Set 1 sample 3.2. All the samples are printed by projecting a blue light circular pattern. The circle area is 0.7838 cm^2 at the DMD plane and 0.4813 cm^2 at the build platform. The blue light intensity is linear to the DMD image grayscale with a full grayscale 255 corresponding to 11.591 mw/cm^2. Note that as the focus of this experiment design is to evaluate IUM capability of capturing the viscoelastic properties of printed parts during various process dynamics, deviations between the design and actual sample geometry might be caused by some improper or non-optimal process settings and occasional dysfunctionality of the in-house DLP system. The potential deformation and dimensional accuracy observed in the printed samples are not within the scope of this experimental study.

Table 3: Design of Experiments for Printing Two Sets of Samples (Set 1: 10-Layer Cylinder, Set 2: 200-Layer Cylinder)

Experimental Group	Sample No.	Exposure time per Layer (Second)	Stage moving speed (mm/s)	Layer Thickness (um)	Exposure Intensity (Grayscale)
Group 1: Varying the stage speed.	1.1	3s	0.1	50	255
	1.2	3s	0.2	50	255
	1.3	3s	0.5	50	255
	1.4	3s	0.7	50	255
	1.5	3s	1.0	50	255
	1.6	3s	1.2	50	255
Group 2: Varying the Layer Exposure Time	2.1	5s	0.2	50	255
	2.2	5s	0.5	50	255
	2.3	5s	0.7	50	255
	2.4	5s	1.0	50	255
	2.5	5s	1.2	50	255
Group 3: Varying the Layer Thickness	3.1	3s	1.0	75	255
	3.2	3s	1.0	25	255
Group 4*: with different light Intensity	4.1 R1	3s	1.0	50	125
	4.1. R2	3s	1.0	50	125
	4.2 R1	3s	1.0	50	63
	4.2 R2	3s	1.0	50	63
*: In Group 4, we have two replications for each process setting.					

3.4 Ex-situ Characterization and Testing Methods

3.4.1 Ex-situ characterization with Fourier Transform Infrared Spectroscopy

It has been found that Degree of Curing (DoC) is directly related to the Young's modulus as the monomers or functional groups crosslink and the resin system undergoes liquid-to-solid transformation. Here in, one approach of measuring Young's modulus for a printed sample is to characterize the DoC value of each printed sample use scientific equipment such as differential scanning calorimetry (DSC) and Fourier Transform Infrared Spectroscopy (FTIR).

In this study, we use FTIR (Bruker Vertex-70LS) for validating the Young's moduli values obtained by IUM. Using FTIR, we obtain the peaks corresponding to the C=C double bond stretching and bending in the cured solid part. During the polymerization reactions, the C=C bonds are opened and converted to single C-C bond in the polymer chains. The DoC for each sample is characterized by the infrared absorbance peaks. Therefore, the degree of conversion is calculated using the absorbance spectrum obtained from FTIR testing result.

Depending on the reacting functional groups the absorbance peaks at different frequencies can be obtained. To calculate the DoC (p) using the absorbance peak difference between cured sample and liquid resin using the following Equation:

$$p = 1 - \frac{\lceil \mathrm{A}_1 + \mathrm{A}_2 \rfloor / \mathrm{A}_3}{([\mathrm{A}_1 + \mathrm{A}_2) / \mathrm{A}_3)_{\mathrm{t}=0}} \tag{3-2}$$

Where, A1 represents a C=C stretching peak at 823 cm^{-1},A2 represents a C=C bending peak, 964 cm^{-1} and A3 a constant peak representing a C=O stretching peak at 1737 cm^{-1}. The denominator (A_1, A_2 and A_3 at t=0) is the peak ratio of the unreacted resin. Each sample were measured with 32 scans at resolution of 4 cm^{-1}. Depending on the different curing pattern used, each sample have three measurement locations one at center and two locations on left and right curbing of the sample. To estimate the Young's modulus from DoC we need to consider the activation energy, glass transition temperature (T_g) and the DoC at the gelation point. Glass transition temperature for the material is calculated with the following equation(Wu 2018):

$$T_g = \frac{E_r}{RIn[g_1(1-p)+g_2]} \qquad \text{3-3}$$

Where E_r is the activation energy of transition from liquid stage to solid stage, R is the gas constant (8.3145 $^{J}/_{K*mol}$), g_1 and g_2 are volume of the cured sample and volume of uncured resin after the printing process, respectively. Once the glass temperature is calculated it is necessary to obtain reaction kinetic equations follow the polymerization steps.

As the polymerization proceeds the polymer chains start to grow and crosslink, cured material passes the gel pointing the crosslinks network results in soild structure with a continuous increase in the material stiffness, there by causing an increase in the Young's modulus. However, the changing in material stiffness and Young's modulus is controlled by reaction kinetics during the polymer propagation and termination steps. Therefore, to evaluate the Young's modulus for each part we need the glass transition temperature calculated by Equation 2-7 and the reaction kinetic constant for polymer propagation step and termination steps, where the kinetic constant k_p

and k_t in polymerization reaction can be calculated with following equations (Wu, J., Zhao, Z., Hamel, C.M., Mu, X., 2018):

$$k_p = A_{Ep} e^{-E_P/RT} \tag{3-4}$$

$$k_t = A_{Et} e^{-E_t/RT} \tag{3-5}$$

where A_{Ep} and A_{Et} are pre-exponential factors, in this study we used a reference value where $A_{Ep} = 28.4 \frac{m^3}{mol*s}$ and $A_{Et} = 8916 \frac{m^3}{mol*s}$, where E_P and E_t are the activation energies for propagation and termination process, R is the gas constant, T is the reaction temperature (for our experiments, it is the room temperature ~22°C). In a typical polymerization reaction, the reaction rate is also influenced by the heat transfer from a heat source to the polymerized material such as fragment vapor process. In our experiments, the effect of heat transfer is negligible, because the polymerization process is caused due to a light source, which took place in a room temperature environment without any additional heat sources. Since the reaction happens without heating, the rate constant will majorly depend on the free volume of the reactant. As the polymerization continues, the free volume of reactant decreases and the mobility for each reacting chemical will reduce, hence the reaction will become a concentration-controlled reaction instead of temperature-controlled reaction. As a result, at room temperature, kinetic constant k_p and k_t are expected to be larger when there is more free volume of the reactant.

As the photo polymerization proceeds, the change in Young's modulus can be evaluated from the following equation (Wang, J., Zhao, C., Zhang, Y., Jariwala, A., & Rosen, D., 2017):

$$E = \frac{1}{(3 * b * k_t[M]k_p[P])} * T_g * exp\left(p - p_{gel}\right) \quad 3\text{-}6$$

Where b is the Boltzmann constant ($1.3806*10^{-23} J/_K$) [M] and [P] are the concentration of monomers and polymer crosslinks during the process, p_{gel} is the DoC at the gelation point for the resin where $p_{gel} = 0.58$. Consider the concentration of the polymer

$$[P] = -2.3\phi_i k_p I \quad 3\text{-}7$$

Where ϕ_i is the quantum yield of initiation in this study we assume the quantum yield as 0.0280 (Tang 2005) and I is the absorbed light intensity (rate of absorption) for the resin.

3.4.2 Ex-Situ Characterization: Dynamic Testing

Another approach to determine the Young's modulus for a printed sample it to perform Nano-dynamic testing to the printed sample. Nanoindentation testing was used to determine the the storage modulus and reduces modulus of the testing sample. It is known that a harmonic frequency of nanoindentation experiments does not have a significant effect on the measured storage and loss moduli of the polymers. (Odegar, G.M., Herrings, H.M, 2005). It provides a direct entry to investigate the viscelatsic behavior of a polymer material, by preforming nanoindentation testing with difference frequency. Following the sample idea in this study frequency sweep nano-indentation testing was performed using a Hysitron TI 950 Triboindenter (Bruker Ltd, Billerica, MA). Viscoelastic behavior is a combination of elastic and viscous behavior where the applied stress results in an instantaneous elastic strain followed by a viscous, time-dependent strain. Once a polymer material experiences elastic deformation where stress increased linearly with strain. After the deformation reach above the yield point it experiences a viscous deformation occurs without an increase of stress and strain. In frequency sweep testing, i.e., the materials mechanical properties vary with the strain excitation frequencies. To evaluate the dynamic behavior of the printed samples, a ramping frequency test (frequency sweep test) with frequencies from 10Hz to 200 Hz is used. At lower frequencies, the material's displacement is dominated by its elastic component, at higher excitation frequencies the viscous component of the material dominates. From the frequency sweep tests, three parameters, namely, reduced modulus E_r, storage modulus E_s, and damping coefficient value C_s need to be deduced, for evaluating the Young's modulus of the printed sample. The storage modulus denotes the polymer sample's ability to store energy elastically and the reduced modulus denotes the polymer sample's ability to dissipate energy. (Franck 2018).

From the frequency sweep test the sample damping C_s is calculated by(Bruker 2014):

$$C_s = F * \frac{\sin(\theta)}{U * \omega} - C_T \tag{3-8}$$

Where F is the dynamic actuation force, θ is phase during the frequency sweep, U is the dynamic displacement ω is the radial frequency and C_T is the transducer damping.

The storage E_s and reduce modulus E_r are directly related to the storage stiffness (k_s) and loss stiffness (k_r) and the contact area A_c during the experiment. The storage stiffness and loss stiffness are defined as(Bruker 2014):

$$k_s = F * \frac{\cos(\theta)}{U} + m_T * \omega^2 - k_T \tag{3-9}$$

$$k_r = \omega * C_s \tag{3-10}$$

Where m_T is defined as the mass of the transducer and k_T is defined as the stiffness of the transducer. The contact area is determined from the following relation(Bruker 2014):

$$A_c = h_c^2 C_0 + h_c C_1 + h_c^{1/2} C_2 + h_c^{1/4} C_3 + h_c^{1/8} C_4 + h_5^{1/16} C_5 + \mathrm{B} \tag{3-11}$$

Where h_c is the contact displacement, and (B) is a machine offset factor that that allows the area function fit to deviate from the origin. Where the C_{0-5} is a system define testing segments during the experiments. The determine contact displacement use the following equation(Bruker 2014):

$$h_c = (h + U) - \varepsilon * (P + F)/k \tag{3-12}$$

Where j is the maximum displacement of material from the original position, $\varepsilon = 0.75$ is defined as a geometric constant related to the testing probes, *P* is the maximum force and *k* is the stiffness of the testing material. Now the storage E_s and reduced modulus E_r can be solved with the following equation:

$$E_s \text{ or } E_r = \frac{k\sqrt{\pi}}{2\sqrt{AC}} \tag{3-13}$$

Where k is calculated as the storage or reduced stiffness to obtain the respective modulus value. With known storage and reduced modulus to analysis the Young's modulus of a polymer-based material we characterized the material Young's modulus E with the following equation

$$E = \frac{1}{2}\left(\frac{1 - v_s^2}{E_s} + \frac{1 - v_i^2}{E_i}\right) \tag{3-14}$$

Where *E* is the Young's modulus, E_s is the storage modulus for the sample, v_s is the sample's Poisson's ratio equals to 0.27, E_i and v_i is the Young's modulus and Poisson's ratio for the indenter tip in this study the tip material is diamond with poisons ratio as 0.07 and the Young's modulus as 1200 GPa.

However, the storage and reduced modulus is concisely related to the loss factor, which is a ratio between the dissipated and stored energy from a dynamic contact experiment. In practice, loss factor can be expressed as follow (Yasser Zare 2019)

$$tan\delta = \frac{E_r}{E_s} \tag{3-15}$$

To calculate the damping ratio based on the damping result we get from Nanoindentation testing using the critical damping C_{crit} occurs at maximum tip displacement and the corresponding average damping C_{ave} obtains at it testing tip oscillatory frequency with following equation:

$$\delta = C_{ave}/C_{crit} \tag{3-16}$$

4.0 Experiment Result and discussion

In this chapter we will discuss findings we have from Degree of Conversion (from FTIR experiments), Young's modulus and damping ratio calculate from ex-situ measurements (Nanoindentation experiments) and in-situ IUM measurements. Set 1 and Set 2 samples DoC results discussed in section 4.1. Comparison between Set 1 and Set 2 samples Young's modulus and Set 1 sample Young's modulus evolution discussed in section 4.2. Characterization of viscoelastic properties with damping ratio and loss factor discussed in section 4.3.

4.1 FTIR Measurement for the Degree of Conversion of Printed Samples

According to the FTIR spectrum we obtained three peaks located at wavenumber 823 cm^{-1},964 cm^{-1} and 1737 cm^{-1} (peak location shown in Figure 10). The first peak indicates a stretching C=C bond, the second peak indicates a strong C=C bond, and the third peak indicates aa C=O stretching peak which used as a constant peak to calculate the degree of conversion for each sample. Results of DoC for each sample at each measurement location using Equation 1 shown in Table 5.

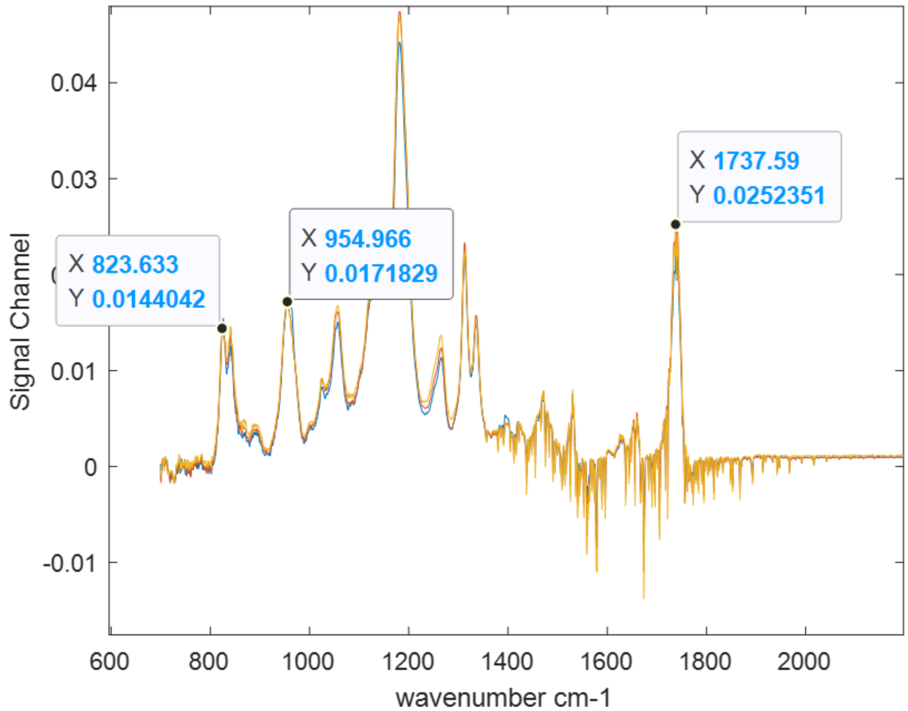

Figure 10 FTIR Spectrum for Set 1 200-Layer Samples

According to the degree of conversion results provides in Table 4, at the center measurement location DoC appears to be the maximum for each sample. Meanwhile we could see the influence of DoC is dominated by the exposure time and light intensity as results shown in Table 4. As we increase the exposure time for each layer, more free radicals will be decomposed form the photo initiator to react with monomers to form more polymer crosslink. However, Group 1 DoC indicates for sample cured with same exposure time for each layer the light intensity for reach layer stays the same thus the reaction kinetic constant will stay as a constant since the reaction kinetic constant is depends on the exposure light intensity.

However, it is not enough to know the DoC for the whole part, to better understand the behavior DoC for each sample at the beginning of the printing process we perform another set of experiments with the sample printing parameters for each sample but only print 10 layers to learn the different in DoC. The results of DoC for sample with 10 layers and 200 layers shown in Table 4. The results of DoC of Set 1 and Set 2 samples at the center measurement location shown in Figure 11.

Table 4: DoC Results of DoC for Set 1 and Set 2 Samples from FTIR Measurement

Experimental Group	Sample No.	Set 1 of 200-Layer Sample	Set 2 of 10-Layer Sample
Group 1: Varying stage speed	1.1	0.244	0.447
	1.2	0.258	0.464
	1.3	0.268	0.47
	1.4	0.292	0.485
	1.5	0.311	0.492
	1.6	0.334	0.504
Group 2: Varying layer curing time	2.1	0.325	0.509
	2.2	0.31	0.513
	2.3	0.34	0.52
	2.4	0.353	0.522
	2.5	0.349	0.524
Group 3: Varying layer thickness	3.1	0.228	0.44
	3.2	0.36	0.609
Group 4: Varying light Intensity	4.1 R1	0.107	0.263
	4.1 R2	0.106	0.265
	4.2 R1	0.205	0.385
	4.2 R2	0.216	0.391

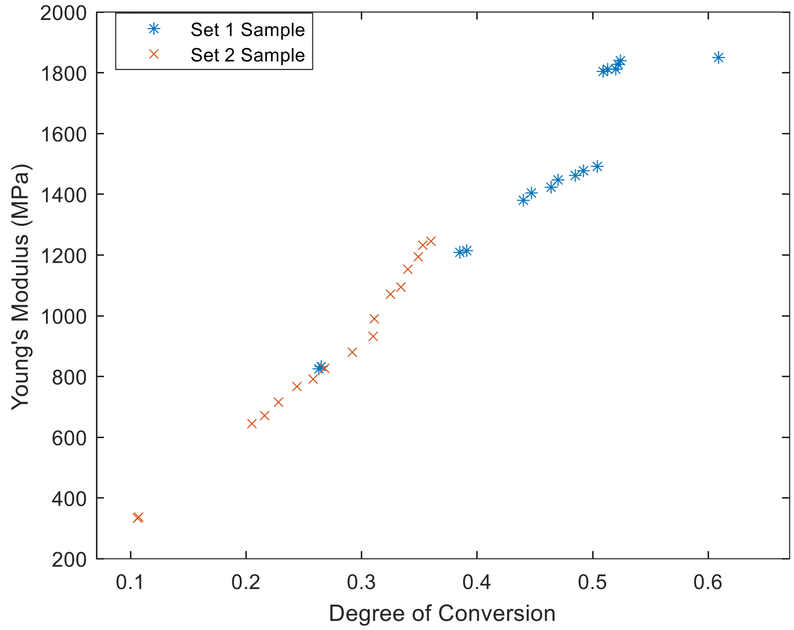

Figure 11 Results of DC DoC for Set 1 and Set 2 Samples Based on FTIR Measurement

As shown in Figure 10 DoC for Set 1 sample with 200 layers are larger than the DoC of Set 2 sample with 10 layers, where DoC at the beginning of printing (as set 2 DoC) process is smaller than the DoC at the end of the printing process(as set 1 DoC). It verifies our idea which during the printing of a new layer curing light is penetrated those the fresh printing layer thus keep solidifies the previous layer thus leads to an increase in the DoC result at the end of the printing process.

However, for groups 2 sample in Set 1 we observed an overcuring problem, occurs at the lower 2mm section of the sample, where experiences a longest total exposure during the experiment as the printing process proceeds. Figure 12 gives an illustration of the over curing in sample (marked with red square) cured with 5 second layer exposure time.

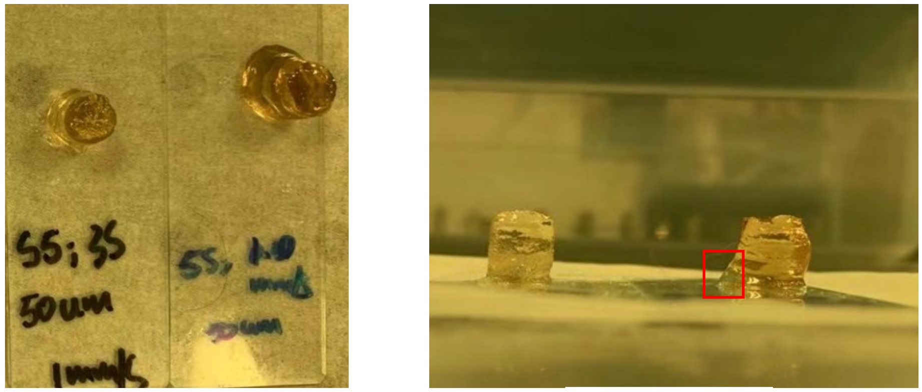

(a) (b)

Figure 12: Sample Cured With Same Stage Speed, Different Exposuretime ((a) top view and (b) side view).

4.2 Measurement of Young's Modulus with IUM and ex-situ Characterization Methods

In this study we employ IUM for evaluating the Young's modulus. The IUM measurements are validated using ex-situ characterization methods, namely, FTIR and Nanoindentation. This section discusses the results obtained using these three methods. Briefly, the three employed methods are:

1. Method 1 should be IUM Use ultrasonic wave velocity and material density to calculated the Young's modulus using using Equation 2-1-Equation 2-2.
2. Method 2 is based on FTIR: Use degree of conversion (calculated from FTIR spectrum peaks), reaction kinetic constants and glass transition temperature to calculate the Young's modulus Equation 3-2-Equation3-7
3. Method 3: is based on nanoindentation: Use Storage modulus and Poisson's ratio from nanoindentation experiemnt to calculate the Young's Modulus using Equation Equation 3-8-Equation 3-14.

For each calculated Young's modulus during the IUM. we first calculate the longitudinal wave velocity for the printed part using Equation 2-1 with the time shift between the reference signal (no-print signal) to the current printing layer. Although, during the printing process as we increase the intermediate part thickness the shifting in wave spectrum also increase which indicates the time traveled through the sample has been increase thus result in an increase in Young's modulus as the printing process proceeds. As an example, the shifting in ultrasonic wave signal between 191st measurements to the 199th measurements shown in Figure 14.

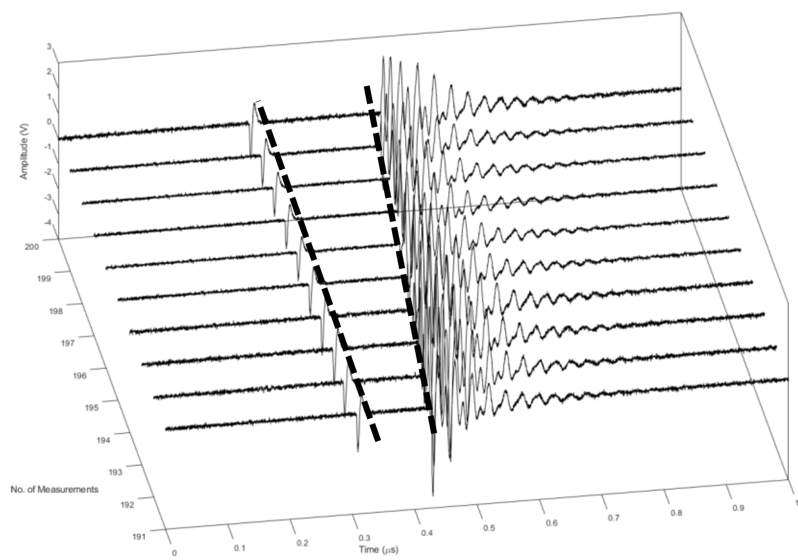

Figure 13: Graph Showing the Measurement Signal Variation for the Last 10 Measurement Layers. The dotted line shows the observed shift in the signal with the increase in layer height

In order to compare the part Young's modulus calculated using IUM method with FTIR based ex-situ method we use the last measurement of IUM method-based Young's modulus since the last measurement represent the Young's modulus of the entire part. Comparison between the

Young's modulus from FTIR based, indentation ex-situ measurements and In-Situ IUM measurements shown in Figure 14. Corresponding evaluated Young's modulus for Set 1 sample shown in Table 5. The IUM error percentage is calculated as per the formula:

$$IUM\ Error\% = (IUM - Ex_{situ})/Ex\_Situ \qquad 4\text{-}1$$

Use IUM value at each set and ex-situ measurement value to find the error percentage. Detailed calculation result between IUM Young's Modulus measurements and ex-situ Young's modulus measurement for Set 1 sample shown in table 5, for Set 2 sample see Appendix table 7 and 8 It is found that the IUM can measure Young's modulus for final-printed part with an accuracy of 91.4% and intermediate part with an accuracy of 94.3%

Table 5: Results of Set1 Sample Young's Modulus From IUM Method and Ex-situ Methods

Experimental Group	Sample No.	Set 1 of 200-Layer Sample		
		In-situ Measurements (IUM) for Entire Part (MPa)	Ex-situ Nanoindentation base Measurements (MPa)	Ex-situ FTIR based Measurements (MPa)
Group 1: Varying stage speed	1.1	1401.318	1413.932	1404.259
	1.2	1417.897	1421.338	1423.091
	1.3	1442.840	1433.036	1447.288
	1.4	1453.293	1440.291	1461.956
	1.5	1461.472	1445.23	1477.349
	1.6	1489.940	1454.685	1491.796
Group 2: Varying layer curing time	2.1	1797.419	1804.883	1804.276
	2.2	1842.849	1836.66	1832.536
	2.3	1849.741	1848.478	1839.716
	2.4	1871.094	1869.942	1867.865
	2.5	1884.095	1878.347	1874.620
Group 3: Varying layer thickness	3.1	1263.810	1257.226	1280.143
	3.2	1887.173	1882.859	1893.144
Group 4*: Varying light Intensity	4.1 R1	896.840	891.801	825.313
	4.1 R2	887.516	872.515	832.515
	4.2 R1	1251.094	1245.02	1208.601
	4.2 R2	1247.849	1250.036	1214.412

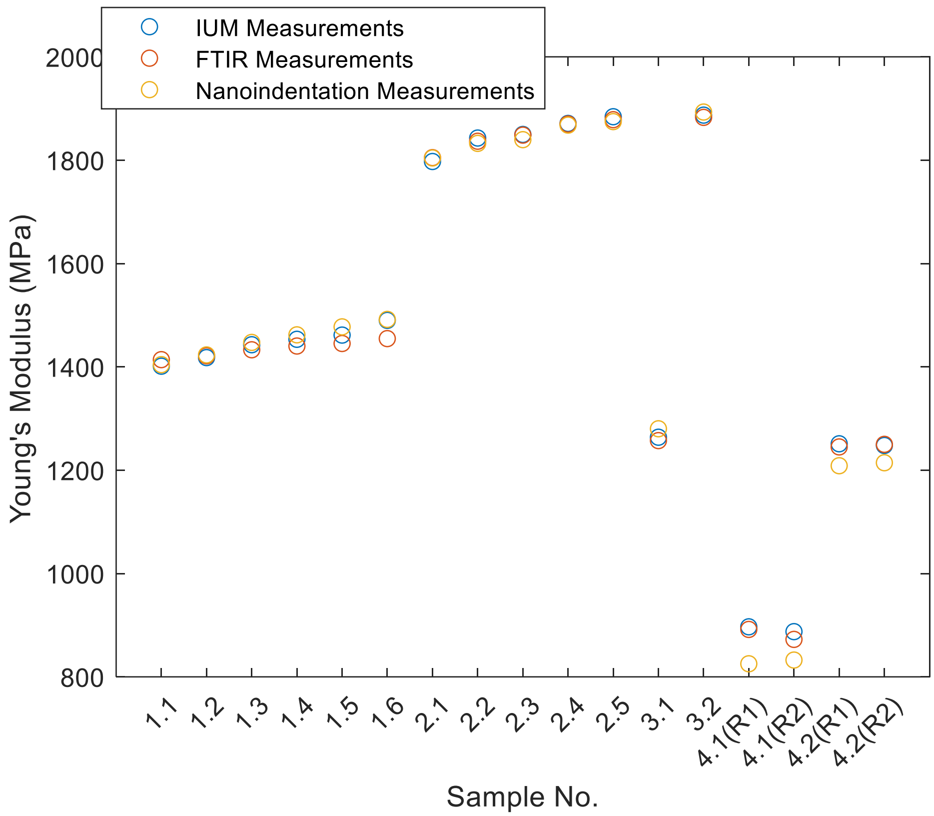

Figure 14: Young's Modulus for Set 1 Samples with Method 1 IUM, Method 2 FTIR based Ex-Situ Measurements, Method 3 Nanoindentation based In-Situ Measurements

However ex-situ measurements Young's modulus results appear to be higher than IUM measurements results, which indicates the possibility of dark curing after the printing process has finished. Dark curing drives polymer chain crosslinks in each sample to be more rigidly order, to further increase the sample stiffness and bring possible volume shrinkage.

To futter demonstrate the ability of our IUM system for during the intermediate part printing Figure 15 shows Young's modulus in result in Set 1200 layer sample, and Set 2 10-layer sample. Where the maximum intermediate part error percentage of Young's modulus between IUM and ex-situ measurements is percentages 5.703 % detailed calculation results see Appendix Table-8.

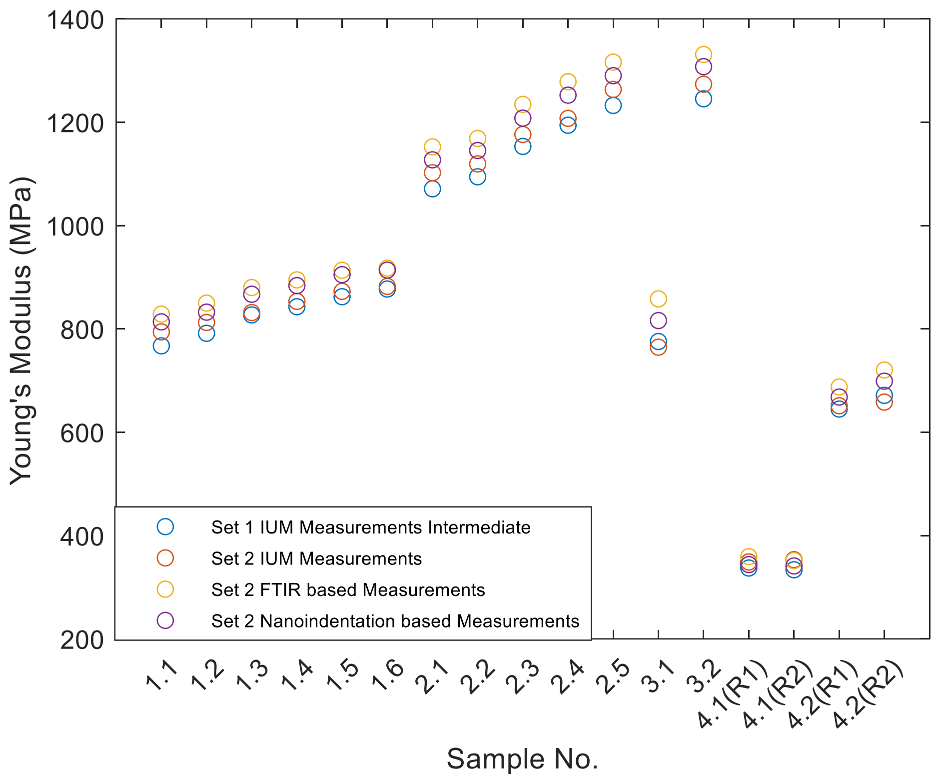

Figure 15: Set 1 IUM Intermediate Measurements, Set 2 IUM Measurements, Set 2 FTIR based Measurements, Set 2 Nanoindentatuon based Measurements.

Based on Young's modulus results calculated from FTIR based ex-Situ measurements we could see the change in Young's modulus for layer curing time at 3 second increase from 1404.259 MPa to 1481.796 MPa, shown in figure 12. Young's modulus for layer curing time at 5 second increased from 1807.276 to 1850.144 with the increase in stage moving speed, shown in Figure 16. As the sample DoC increase Young's modulus increasing due to a higher C=C bond to C-C bond conversion in the sample.

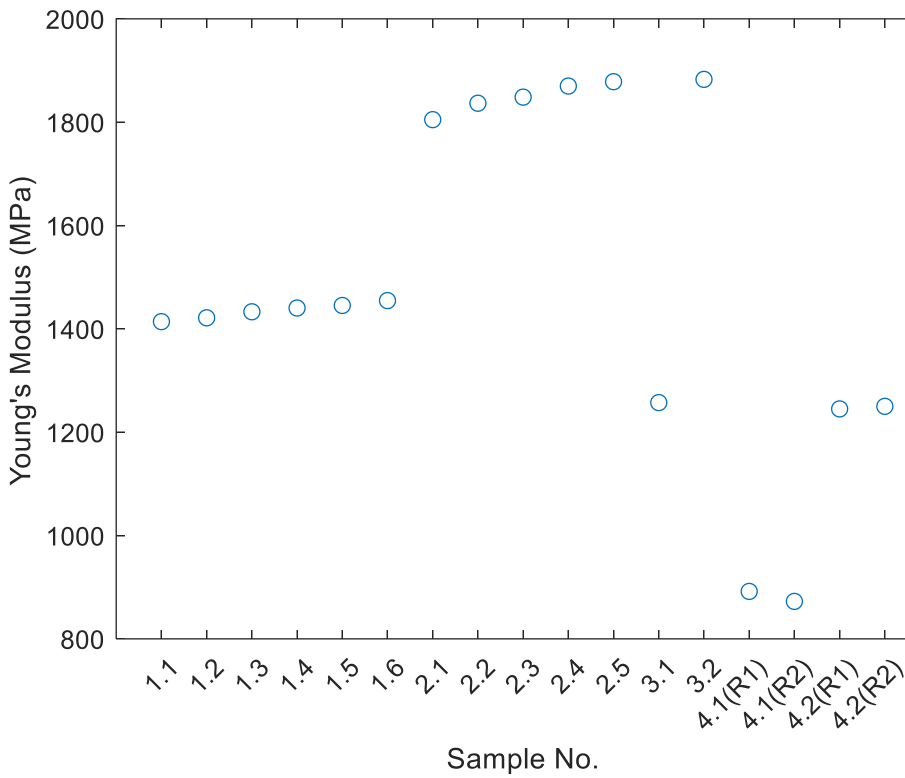

Figure 16: Results of Young's Modulus using FTIR based Ex-situ Measurement For Set 1 Samples

Method 3 uses Nanoindentation based ex-situ measurements with the storage modulus, and Poisson's ratio to calculate the Young's modulus of each sample using equation 18. From Nanoindentation experiment we want to consider the relation between displacement and frequency first shown in Figure 17 to understand the how sample displacement varies according to different tip frequency. In frequency sweep method, under different frequency the indenter tip will leads to a corresponding displacement range to this frequency.

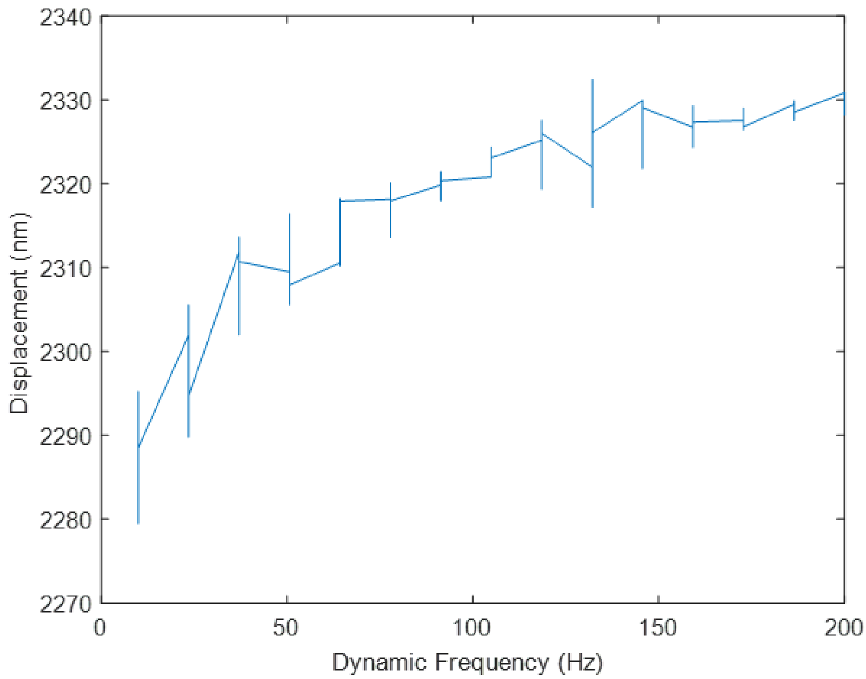

Figure 17: Nanoindentation Measure Sample Displacement at Different Indenter Tip Excitation Dynamic Frequency

To calculate the Young's modulus from nanoindentation measurements result, we use maximum storage modulus of the sample, when the indenter tip contacts with the testing sample. It represents the storage modulus of sample at the last layer after the printing process is finished. Result of Storage modulus and calculated Young's modulus shown in Table 6

Table 6: Nanoindentation Measured Storage Modulus and Calculated Young's Modulus for Set 1 Samples

Experimental Group	Sample No.	Set 1 of 200-Layer Sample	
		Storage Modulus (MPa)	Young's Modulus (MPa)
Group 1: Varying stage speed	1.1	3278.448	1413.932
	1.2	3261.365	1421.338
	1.3	3234.741	1433.036
	1.4	3218.449	1440.291
	1.5	3207.450	1445.230
	1.6	3186.602	1454.685
Group 2: Varying layer curing time	2.1	2568.311	1804.883
	2.2	2523.875	1836.660
	2.3	2507.739	1848.478
	2.4	2467.861	1878.347
	2.5	2478.954	1869.942
Group 3: Varying layer thickness	3.1	3687.088	1257.226
	3.2	2488.380	1862.859
Group 4: Varying light Intensity	4.1 R1	5197.909	891.801
	4.1 R2	5312.807	872.515
	4.2 R1	3723.234	1245.020
	4.2 R2	3708.294	1250.036

Both method 2 and method 3 could only discuss the Young's modulus of the sample after the printing process is finished. To clearly see this Young's modulus difference between the printing process we need to use method 1 to investigate the real time Young's modulus for each sample after a new layer printed.

Evolution of Young's modulus for each Set 1 samples shown in Figure 18(a)-(e) appears to have three stages (Detailed calculation results for each sample at each measurement shown in Appendix A Table1-4). Start with stage 1 the developing stage where the Young's modulus corresponds to the first 10-20 layers during the printing process. As the printing process proceeds, Young's modulus reaches to a propagating stage, stage 2 where a rapid increase in Young's modulus occurs. In stage 2, Young's modulus experiences a rapid increase until it reaches to stage 3 steady state. In stage 3, The increase in Young's modulus slows down and trending to a steady state as the printing process proceeds to finish.

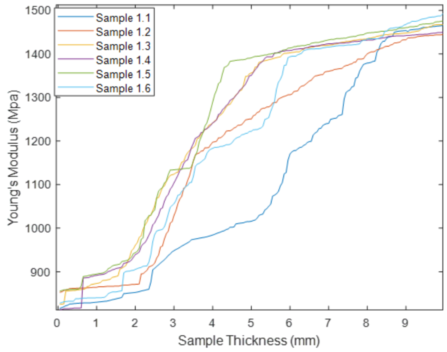

(a)

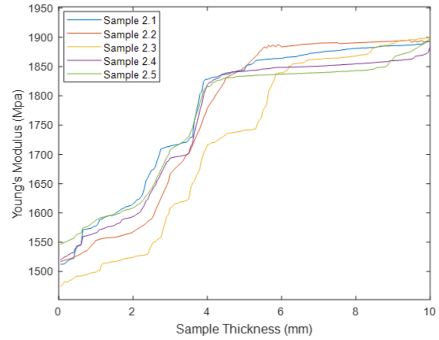

(b)

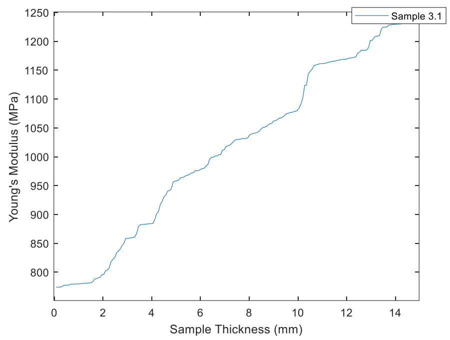

(c)

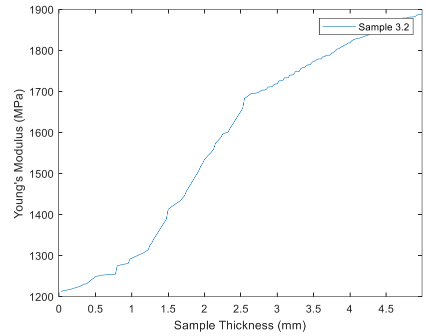

(d)

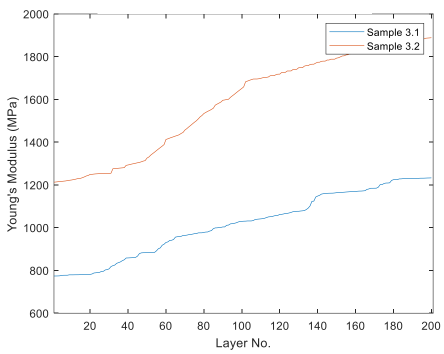

(e)

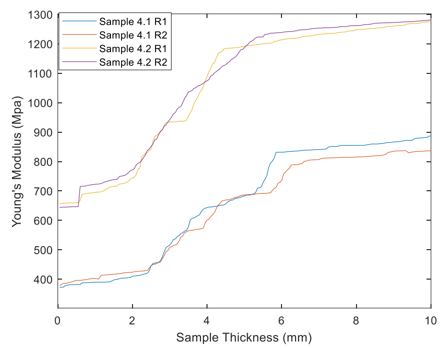

(f)

Figure 18: (a) In-situ IUM Measured Young's Modulus After Printing Each Layer. Group 1: Varying Stage Speed. (b) In-situ IUM Measured Young's Modulus After Printing Each Layer. Group 2: Varying Layer Exposure time. (c) In-situ IUM Measured Young's Modulus After Printing Each Layer. Group 3, Sample 3.1: Varying Layer Thickness-Layer thickness 75um. (d) In-situ IUM Measured Young's Modulus After Printing Each Layer. Group 3, Sample 3.1: Varying Layer Thickness-Layer thickness 25um (f) In-situ IUM Measured Young's Modulus After Printing Each Layer. Group 3, Varying Layer Thickness With Horizontal Axis as Number of Layer (e) In-situ IUM Measured Young's Modulus After Printing Each Layer. Group 4: Varying Layer Curing Light Intensity.

The evolution of Young's modulus involves the change in polymer and monomer concentration as we change the printing condition for each sample. As mentioned earlier in section 2.2.3 Young's modulus is closely related to the chemical reaction during the printing process which depends on the concentration of reacting monomer in the propagation step and the concentration polymerized polymers in the termination step. To verify the Young's modulus at the developing stage we compare the result between sample in Set 1 and Set 2, where the Young's modulus from Set 2 samples have value closer to the intermediate Young's modulus (corresponding to 10 printed layers) from Set 1 see Appendix table 7.

As we increase layer thickness, larger quantity of photo initiator decomposed thus allow a more rapid DoC from monomer to polymer, thus increase Young's modulus for each layer measurement. Typically, for all samples as we increase the exposure time, we are allowing more free radicals to react with the monomers. In this case, with the increase in exposure time, we are increasing the concentration of monomer is the propagation process, at the same time allows more polymers to crosslink therefore increase the Young's modulus for the printed part. Similarly, the change in the sample's Young's modulus is directly proportional to the light intensity (I). As we change the light intensity with different grayscale values for the blue light, we modulate the actual light intensity I, reaching the resin surface. Which further modulates the kinetic constant during the propagation step and the concentration of polymerized polymer at the termination step, thus leading to the appropriate Young's modulus of the printed parts. However, stage moving speed is not a key parameter to determine the Young's modulus, since sample cured with same exposure time the reaction kinetic constant stays constant, but as stage moving speed increases it allow resin underneath to flow faster thus allow more unreacted photo-initiator prepared to be decomposed in the decomposition process to produce more free radicals during the next layer exposure at the curing site therefore give a larger Young's modulus for the printed part.

4.3 Characterization of Viscoelastic Properties with IUM and Ex-situ Methods

To find the damping ratio and loss factor of the printing sample we apply logarithmic decrement method to last measurements of each sample from the in-situ IUM measurements (method 1) using Equation 2-3 and Equation 2-4. To find damping ratio and loss factor from Nanoindentation based measurement (method 2) using Equation 3-15 and Equation 3-16.

Based on IUM in-situ measurements, the damping ratio is calculated with 4 consecutive peaks shown in Figure 6 at the last layer using Equation 2-4 where the value of damping ratio between each consecutive peak shown in Figure 19.

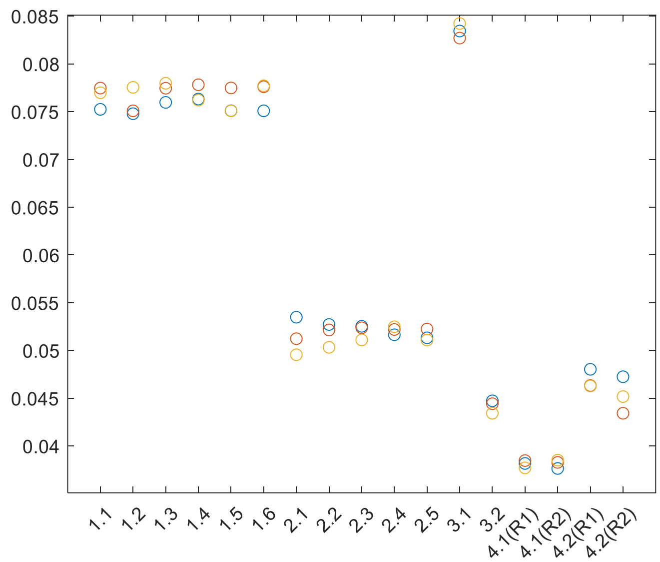

Figure 19: Damping Ratio for Method 1 based on In-situ Measured Damping Ratio

Based on the ex-situ indentation-based measurement, indenter tip causes a range of displacement on the testing materials, thus to evaluate the damping ratio for each sample we use the average damping result measured where the indenter tip oscillates at 10 Hz. At low frequency range sample higher value of storage modulus representing the testing sample will behavior more elastic.

We find the average damping of the material from Nanoindentation based measurements for each sample varies between 0.000147 kg/s to 0.000518 kg/s depending on the printing condition. To compare the damping ratio results from Nanoindentation testing and IUM measurements, we compare the trends damping ratio corresponding to the printing condition. Average value of damping ratio calculates from IUM measurements shown in Figure 20 (a), average damping to calculated from Nanoindentation measurements shown in Figure 20(b).

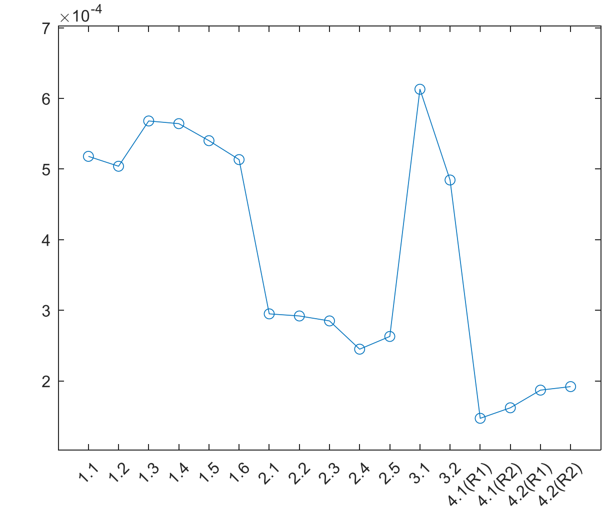

Figure 20: (a) Damping Ratio From Method 1 IUM In-Situ Measurement

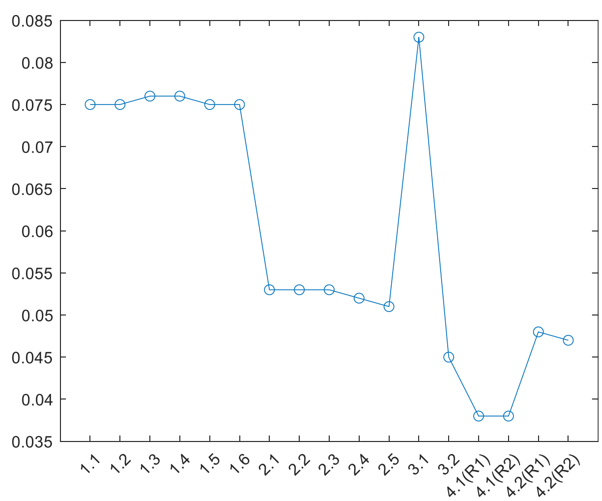

Figure 20 (b) Damping Ratio From Method 2 Indentation Measurements

Figures 20 (a) and (b) show that the relation between damping ratio values obtained from IUM and Nanoindentation methods, respectively, showing a similar trend. Based on these results, it can be concluded that the damping ratios obtained from our IUM method are in agreement with the ground truth values obtained from Nanoindentation. Once increase the curing time, layer thickness and light intensity, the corresponding damping ratio and damping decreases detailed calculation results shown in Appendix A Table 5.

To calculate the loss factor for our material we apply two different methods. Method 1 using Equation 2-5 with calculated damping ratio from IUM measurement. Method 2 using Equation 2-20 with Nanoindentation testing measured storage and reduced modulus. For polymer material loss factor is a ratio of material viscos to effects. Calculated loss factor from IUM measurements and Nanoindentation testing shown in Figure 21, corresponding calculation result of loss factor provides in Appendix A, Table 6.

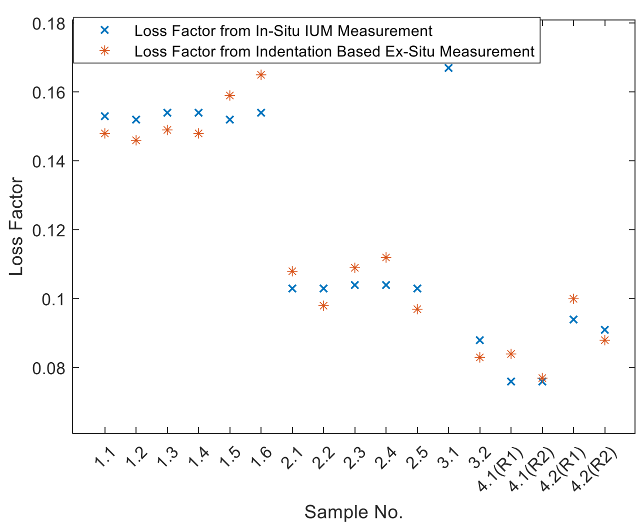

Figure 21: Loss Factor from Method 1 (IUM) Measurements and Method 2 (Indentation Based Ex-situ Measurement)

For common polymer material such as polypropylene, polystyrene, and polyethylene the Loss factor for each polymer ranges at 0.17 ± 0.006, 0.16 ± 0.007, and 0.19 ± 0.008 with Atomic Force Microscopy (AFM) measurements.(Yablon 2015). According to the results of damping ratio and loss factor of our samples by method 1 and 2, a larger value indicates higher degree of viscous behavior of the printed material. Relation between printing condition and damping ratio shows us, once sample cured with shorter layer exposure time, faster stage moving speed and larger layer thickness is results in a higher value of loss factor and damping ratio. It indicates that those sample behaviors more viscos with a loosely order polymer chain crosslinks. In Nanoindentation frequency sweep test, at higher frequencies, the material damps out as much energy as it stores and returns elastically. Relation between loss factor and testing frequency during the indentation experiment shows that at same frequency oscillation loss factor appears to be a constant. Consider the relation between loss factor and frequency, loss factor increases sharply with tip excitation frequency increases over the testing domain. This implies that the material is approaching (in spectral domain) a phase transition detailed in section 4.4.

4.4 Applying IUM to Understand the Effects of Process Parameters on the Viscoelastic Properties of Being-printed Parts

Result of Young's modulus from three methods appears to have a similar relation as we increase the layer exposure time, stage moving speed, and layer thickness will result in a higher Young's modulus due to a more an increase in sample stiffness with an increase in DoC. It was caused by the degree of conversion increase as the printing process proceeds Results of loss factor and damping ratio indicate that for our cured polymer material, For polymer materials, there exist various unique states. These regions are typically referred to as the rubbery transition and glassy regions(Y. Zhang 2013). From flow to glassy region the material changes from soft gel state to solid state. At rubbery region polymer chains are loosely ordered which would result in a soft gel material with lower Young's modulus, in the glassy region polymer chains are rigidly ordered resulting in a stiff solid material with higher Young's modulus(Pritz 2001). Figure 17(a)-(e) shows we increase the layer curing time, stage moving speed, layer thickness and exposure light intensity. We observe changes in the Young's modulus appears to have a more rapid increase in the propagation stage, by allowing more monomer to react with free radicals to form polymer chains leads polymer concentration in each layer to increase. As the printing process proceeds the total exposure time for the part increases which drives polymer chains in each layer to be more rigidly ordered, thus increase material stiffness leads to a higher steady state Young's modulus.

At the same time the viscoelastic materials behave differently from rubbery stage to glassy stage. In the rubbery region, the material has a lower stiffness, and lower damping. In the transition region, the material appears to have viscoelastic response, where the damping performance changes evidently compared to the glassy and rubbery phases shown in Figure. 22.

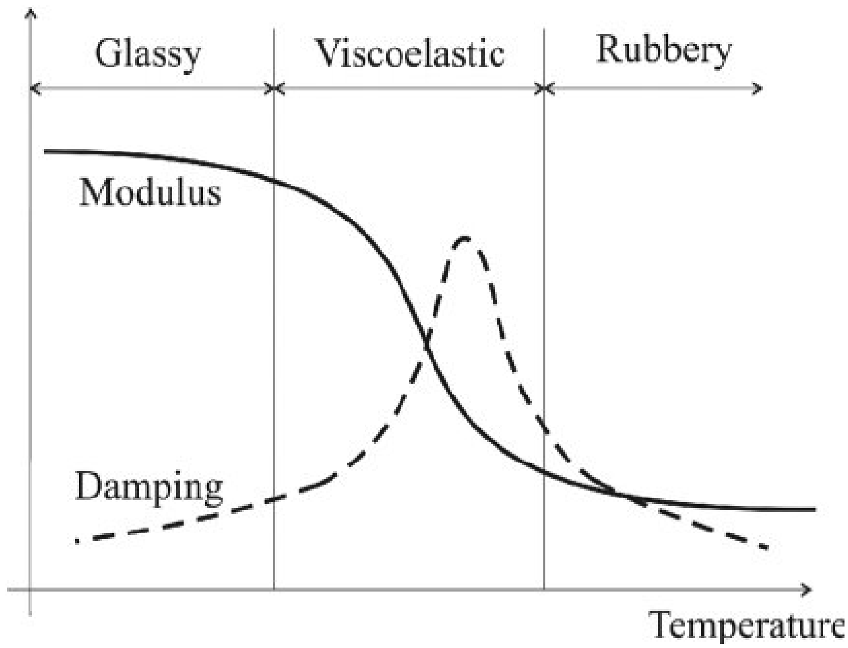

Figure 22: Young's modulus and damping vs temperature of a polymer (Y. Zhang 2013)

In the glassy region the polymer chains are rigidly ordered results in a stiff material, in this region the damping is relative higher.(Macoice 2010) To discuss the loss factor of polymer material, high loss factor indicates an intensive rubber to glass transition phenomenon corresponds with a large modulus dispersion.(Pritz 2001). Normally under frequency controlled dynamic testing it exists at least one peak in loss factor indicates polymer material behavior evolves from more elastic behavior to more viscous behavior.

For our material it results in a reduction of damping as the excitation frequency increases. A representative plot showing this observed trend is shown in Figure. 23 Once the testing frequency increase material appears to be more viscous gives a relative lower damping by considering the modulus of a viscoelastic material as a complex quantity. At higher frequency material appears to have a higher reduced modulus which represent the viscous part of the complex modulus material dominates therefore results in a more viscous behavior. At lower frequency with a higher storage modulus and a lower reduce modulus which represent the elastic part of the complex modulus dominates therefore results in a more elastic behavior. In frequency sweep testing at each testing frequency material damping varies.

Loss factor from Nano indentation experiments shown in Figure 23, shows a correspondence increase in loss factor as the tip excitation frequency increase, with the increase in reduced modulus. As the Loss factor increases the elastic component of the material loss influence in the corresponding complex modulus where it's corresponding storage modulus decrease. Once the loss factor is greater than 1 reduced modulus increase and dominate the complex modulus of the sample thus the viscous component of the material prevails.

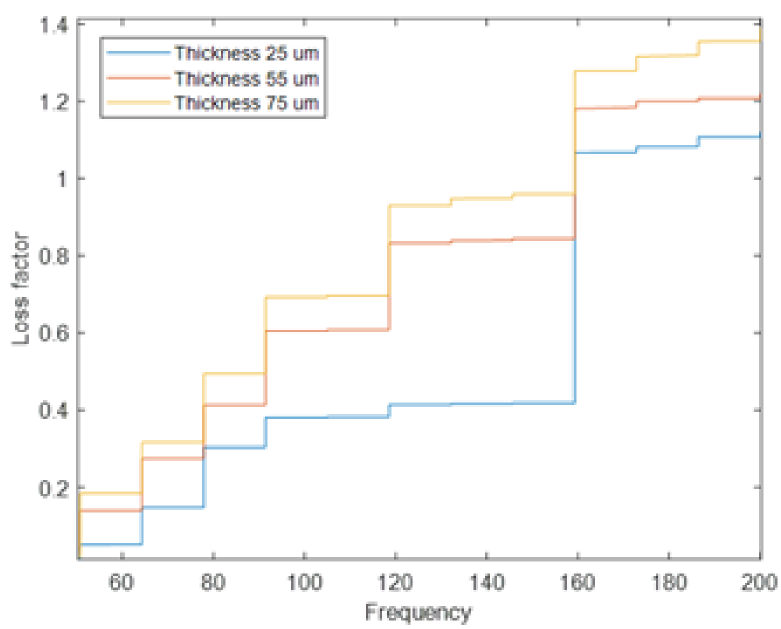

Figure 23: Calculated Loss Factor for Samples with Different Layer thickness with Indenter Tip Excitation Frequency

From the results of loss factor for each sample shown in Figure 21, the difference in loss factor is dominated by the change of light intensity, layer exposure time, and layer thickness. With increase in these three parameters, it allows the polymer chain to become more rigid thus it causes a decrease in loss factor which indicates the printed sample appears to more elastics. As Nanoindentation results verifies sample with more rigidly order polymer crosslink would give a smaller reduced modulus value in the calculation of loss factor, thus leads to a lower loss factor.

5.0 Conclusions and Future Directions

5.1 Conclusion

This work presents the first-ever in-situ ultrasonic measurement (IUM) instrument for PAM process monitoring. Two sensing modalities are demonstrated with the developed in-situ ultrasonic monitoring system to measure Young's modulus and infer damping ratio of printed parts throughout a DLP process. Experimental study is performed to exemplify that the IUM method can probe the elastic modulus of just-printed part in situ during the printing process, providing information on time-dependent resin conversion or crosslinking density. Meanwhile, the IUM signal can also capture the printed part's viscoelastic damping behavior, indicating gelation-dependent swelling or shrinkage behaviors. Standard scientific measurement and testing including FTIR and Nanoindentation is conducted to validate the IUM analysis results. As the final printed part's modulus and damping coefficient are directly compared and correlated with the offline measurement results, it is reasonable to extrapolate this validation for the intermediately printed part's properties measured by IUM (note: there is no in-situ standard scientific equipment to corroborate directly the IUM approach). Experimental results show that the IUM data and analysis results reflect changes in process conditions such as different exposure intensity and time, layer thickness, and build stage speed. The pattern of dynamically evolving elastic modulus measured by IUM agrees well with modeling calculation reported in literature. This work opens a new in-situ monitoring approach, which is cost-effective and non-destructive, to gain rich insights about PAM process dynamics, as well as establishes a new framework of elucidating process-property relationship during PAM. The developed IUM system and method along with the experimental results will assist researchers to develop advanced process control strategies, which enable 3D and 4D printing of sophisticated products such as soft robots that require localized manipulation of mechanical properties.

5.2 Recommendation for Future Work

In this study the IUM system has a limitation with the minimal detectable thickness as 305.7 um to have more accurate result it is recommended to use improve the IUM system with sensor have higher frequency (pulser receiver maximum excitable ultrasonic pulse: 35MHz). We also suggest to evaluate the loss factor evolution for each layer to better understand the viscoelastic behavior of our printed polymer material.

In this study we only measure the corresponding data error percentage but uncertain analysis needs to be performed in the context of IUM measurements including certainty of measured Young's Modulus, damping ratio and loss factor. In this study we measure simple geometry, in order to apply IUM to complex geometries more advanced analytics needs to be developed such as real time layer thickness monitoring.

Appendix A Table of Related Calculation Results

Appendix Table 1: Results of Young's modulus From IUM Method in Group 1 Samples

Sample Thickness (mm)	Young's Modulus (MPA) Sample 1.1	Young's Modulus (MPa) Sample 1.2	Young's Modulus (MPa) Sample 1.3	Young's Modulus (MPa) Sample 1.4	Young's Modulus (MPa) Sample 1.5	Young's Modulus (MPa) Sample 1.6
0.05	816.087	852.821	825.273	813.291	855.448	828.241
0.1	817.766	854.038	825.522	813.390	857.141	829.423
0.15	819.646	856.780	826.318	814.956	858.477	831.026
0.2	821.926	857.967	855.389	815.127	858.713	831.497
0.25	823.205	859.051	855.670	815.141	858.896	831.959
0.3	825.764	861.397	856.212	815.366	859.206	831.959
0.35	826.041	861.486	856.637	815.639	859.227	832.417
0.4	826.637	861.770	856.970	816.255	859.245	832.417
0.45	827.109	861.915	857.264	816.326	859.260	837.704
0.5	827.410	862.268	858.364	816.461	859.816	838.115
0.55	827.676	862.282	858.677	816.609	860.801	838.249
0.6	828.031	862.410	859.098	816.861	867.719	838.378
0.65	828.184	862.542	859.712	885.472	888.837	839.309
0.7	828.217	862.783	860.657	886.044	889.697	839.309
0.75	828.241	862.945	865.921	886.376	890.169	839.662
0.8	828.272	863.305	866.674	886.895	891.691	839.900
0.85	828.732	863.689	870.464	889.085	892.350	839.900
0.9	829.212	864.051	871.311	889.637	893.417	839.972
0.95	829.572	864.269	872.231	891.174	893.865	839.994
1	830.012	864.334	872.995	891.669	894.550	840.192
1.05	830.572	865.476	873.707	892.744	895.735	840.215
1.1	831.026	865.644	875.401	893.224	896.132	840.215
1.15	831.497	865.692	879.944	893.760	896.904	840.848
1.2	831.959	865.823	880.210	894.767	898.574	841.195
1.25	832.417	866.219	880.826	896.986	901.458	844.442
1.3	833.333	866.287	881.789	900.708	907.246	849.580
1.35	834.409	866.543	882.589	901.439	909.135	851.896
1.4	835.685	866.626	887.056	904.385	913.144	853.371
1.45	836.603	866.753	887.892	905.246	914.795	853.781
1.5	837.736	866.884	889.197	907.420	915.647	853.784

Appendix Table 1 (continued)

1.55	838.801	866.948	890.270	908.235	916.433	854.660
1.6	839.747	867.331	905.905	909.176	917.561	855.599
1.65	841.209	868.781	907.877	910.714	923.409	856.004
1.7	849.572	869.164	911.031	919.239	924.296	897.331
1.75	850.012	869.173	913.891	920.102	925.194	900.372
1.8	850.572	869.341	923.267	921.615	926.494	901.139
1.85	851.026	869.869	932.743	923.265	929.436	901.334
1.9	851.497	870.625	948.252	927.050	933.620	902.837
1.95	851.959	870.778	952.726	933.398	941.676	903.253
2	852.417	871.060	960.980	939.323	943.723	905.287
2.05	853.333	871.187	966.815	941.765	946.677	907.155
2.1	854.409	872.038	978.925	945.352	954.436	908.912
2.15	855.685	894.927	982.292	958.146	974.318	909.818
2.2	856.603	895.562	997.985	963.682	977.878	912.565
2.25	857.736	899.426	1007.327	967.019	1017.392	912.944
2.3	858.801	903.175	1013.686	974.402	1021.671	913.095
2.35	859.747	910.947	1025.861	984.090	1028.836	921.771
2.4	876.417	912.806	1030.263	992.818	1029.795	939.805
2.45	904.393	915.028	1040.226	1007.712	1037.392	969.223
2.5	907.951	919.828	1051.458	1012.315	1041.671	985.453
2.55	912.091	931.060	1069.670	1021.443	1068.836	993.366
2.6	915.868	938.253	1070.061	1029.340	1084.907	995.001
2.65	919.927	956.674	1081.906	1043.973	1089.795	996.025
2.7	923.785	959.051	1093.467	1046.429	1092.933	997.233
2.75	927.394	975.005	1096.793	1061.337	1103.740	1002.962
2.8	931.970	987.038	1107.193	1071.766	1107.781	1015.246
2.85	937.185	993.144	1115.124	1077.298	1123.144	1032.640
2.9	940.732	1011.550	1121.009	1089.281	1133.224	1047.580
2.95	945.626	1014.927	1122.661	1095.052	1133.581	1051.984
3	948.351	1029.281	1123.878	1103.952	1134.024	1056.196
3.05	951.075	1040.195	1127.200	1112.268	1134.478	1063.708
3.1	953.199	1056.412	1128.691	1121.346	1134.958	1075.611
3.15	955.902	1067.038	1140.421	1132.398	1135.242	1076.765
3.2	958.948	1073.144	1151.509	1136.155	1135.316	1084.535
3.25	961.177	1091.550	1153.150	1148.312	1136.804	1088.575
3.3	963.813	1094.927	1165.386	1154.430	1137.114	1095.762
3.35	966.321	1109.281	1173.059	1156.734	1137.208	1097.794
3.4	969.013	1120.195	1177.887	1170.908	1137.330	1104.297
3.45	973.394	1136.412	1182.338	1184.847	1141.136	1105.108
3.5	974.134	1154.442	1185.388	1194.491	1153.740	1118.436
3.55	975.187	1167.883	1189.730	1206.142	1166.398	1141.668

Appendix Table 1 (continued)

3.6	975.963	1170.953	1205.207	1208.809	1176.348	1146.994
3.65	976.780	1172.497	1207.204	1211.558	1197.729	1148.555
3.7	977.706	1176.879	1215.724	1219.303	1208.719	1152.055
3.75	978.517	1177.512	1219.859	1220.613	1219.624	1155.770
3.8	979.329	1184.576	1226.200	1226.672	1234.495	1159.218
3.85	980.150	1184.581	1228.418	1228.513	1241.663	1171.661
3.9	981.621	1185.090	1236.095	1231.834	1255.942	1178.016
3.95	982.704	1191.851	1238.128	1235.929	1272.069	1181.303
4	984.343	1197.368	1241.348	1241.646	1289.603	1183.341
4.05	985.790	1198.292	1246.089	1244.450	1306.077	1185.385
4.1	987.872	1199.551	1249.414	1248.555	1316.897	1185.510
4.15	989.342	1207.255	1256.610	1260.863	1332.009	1185.965
4.2	990.984	1207.386	1259.693	1263.387	1335.618	1187.778
4.25	992.840	1210.424	1263.594	1271.744	1353.715	1187.813
4.3	994.094	1214.862	1270.628	1275.659	1368.821	1189.279
4.35	996.874	1222.650	1278.128	1281.377	1371.113	1191.428
4.4	998.104	1223.391	1282.957	1285.333	1374.565	1191.564
4.45	1002.138	1223.485	1284.299	1293.213	1382.999	1192.568
4.5	1002.229	1225.951	1291.208	1296.280	1383.755	1196.065
4.55	1002.677	1229.903	1299.258	1298.964	1384.379	1202.103
4.6	1009.699	1231.718	1305.752	1304.615	1385.220	1206.145
4.65	1010.550	1236.071	1310.106	1309.685	1385.685	1208.553
4.7	1011.321	1236.359	1315.015	1316.887	1386.228	1209.744
4.75	1011.831	1237.595	1317.335	1320.515	1386.857	1214.268
4.8	1012.318	1242.733	1329.219	1324.897	1386.916	1215.226
4.85	1014.290	1248.576	1348.326	1330.549	1387.593	1217.434
4.9	1015.050	1249.446	1348.425	1339.819	1390.039	1218.058
4.95	1015.151	1250.452	1354.315	1349.738	1390.092	1222.002
5	1015.881	1250.542	1356.339	1350.698	1390.974	1222.249
5.05	1017.460	1258.077	1358.161	1357.493	1392.950	1225.835
5.1	1018.627	1259.845	1369.659	1363.743	1394.157	1226.039
5.15	1023.053	1265.614	1370.442	1368.850	1394.480	1226.162
5.2	1029.372	1266.864	1380.672	1376.354	1394.668	1228.307
5.25	1031.245	1273.242	1381.824	1379.905	1395.840	1230.132
5.3	1032.333	1275.127	1383.627	1383.632	1396.350	1234.195
5.35	1041.595	1275.464	1384.554	1390.047	1397.784	1249.353
5.4	1044.830	1278.332	1385.298	1393.143	1397.848	1251.275
5.45	1050.099	1278.409	1386.766	1393.194	1399.398	1253.693
5.5	1054.810	1280.959	1387.564	1393.263	1399.721	1268.046
5.55	1073.447	1287.207	1388.977	1393.496	1400.945	1279.209
5.6	1075.752	1288.580	1390.240	1402.219	1401.144	1291.343

Appendix Table 1 (continued)

5.65	1078.850	1288.704	1391.439	1402.337	1402.059	1319.004
5.7	1084.255	1296.296	1392.458	1403.614	1402.215	1334.821
5.75	1096.640	1298.721	1393.078	1406.308	1402.550	1341.480
5.8	1104.540	1300.810	1398.614	1406.314	1408.208	1351.955
5.85	1124.718	1302.576	1401.373	1406.528	1409.146	1373.613
5.9	1127.617	1303.916	1401.487	1407.633	1409.707	1374.335
5.95	1156.253	1306.121	1401.978	1407.702	1413.126	1391.272
6	1170.436	1306.122	1402.278	1407.852	1413.570	1393.612
6.05	1175.214	1307.807	1403.306	1408.310	1414.302	1394.621
6.1	1178.004	1313.511	1403.732	1410.072	1416.438	1394.676
6.15	1178.130	1314.507	1404.645	1410.604	1416.684	1394.779
6.2	1181.984	1315.268	1404.828	1411.018	1418.037	1398.072
6.25	1185.060	1322.442	1404.984	1411.608	1418.228	1399.536
6.3	1185.897	1326.225	1408.755	1411.735	1418.896	1401.386
6.35	1189.810	1326.849	1410.485	1412.164	1419.084	1407.352
6.4	1191.991	1330.086	1413.842	1413.986	1419.399	1408.942
6.45	1196.819	1333.800	1413.924	1414.311	1421.219	1410.164
6.5	1198.854	1337.730	1414.039	1416.481	1421.238	1410.958
6.55	1199.418	1339.395	1415.298	1417.490	1424.545	1411.411
6.6	1213.780	1345.177	1415.559	1417.721	1425.224	1411.560
6.65	1218.433	1349.432	1417.460	1417.890	1426.022	1411.684
6.7	1221.150	1350.025	1417.513	1418.697	1426.329	1411.736
6.75	1228.542	1351.289	1417.982	1418.923	1426.466	1411.852
6.8	1229.247	1352.287	1418.877	1420.326	1427.913	1412.628
6.85	1235.736	1352.535	1418.977	1421.192	1428.674	1413.793
6.9	1238.387	1358.514	1419.026	1421.683	1430.192	1414.318
6.95	1239.936	1359.710	1419.354	1422.735	1431.053	1415.452
7	1240.427	1360.176	1419.662	1423.319	1432.376	1415.592
7.05	1249.881	1361.232	1420.317	1423.504	1433.042	1416.151
7.1	1250.874	1362.065	1420.861	1423.614	1433.077	1417.042
7.15	1251.981	1364.489	1422.458	1424.333	1433.777	1417.650
7.2	1252.483	1364.712	1422.798	1424.648	1435.032	1418.410
7.25	1258.088	1365.906	1424.050	1424.649	1435.276	1418.823
7.3	1259.480	1366.257	1426.042	1424.668	1435.330	1418.905
7.35	1260.885	1366.934	1426.894	1424.896	1435.775	1419.150
7.4	1295.920	1371.505	1427.076	1424.898	1436.100	1419.198
7.45	1311.361	1373.299	1428.607	1425.588	1436.153	1419.936
7.5	1315.045	1374.066	1428.664	1425.604	1438.083	1420.389
7.55	1317.155	1376.374	1429.029	1426.568	1438.891	1420.623
7.6	1324.243	1377.323	1429.977	1427.849	1439.566	1420.703
7.65	1325.769	1380.686	1431.441	1428.270	1439.981	1421.314

Appendix Table 1 (continued)

7.7	1344.260	1380.989	1431.487	1428.458	1440.223	1421.469
7.75	1346.254	1387.952	1432.278	1428.718	1442.288	1422.218
7.8	1360.033	1388.207	1433.191	1429.156	1443.291	1423.128
7.85	1368.184	1388.230	1433.306	1430.661	1443.905	1429.289
7.9	1375.582	1388.889	1433.531	1431.349	1444.168	1431.272
7.95	1377.684	1395.349	1433.587	1431.461	1446.618	1431.272
8	1379.030	1400.299	1434.998	1431.692	1448.032	1434.621
8.05	1379.398	1402.747	1436.260	1431.742	1448.486	1434.621
8.1	1380.814	1404.494	1436.422	1432.018	1448.783	1434.676
8.15	1382.889	1404.617	1437.816	1432.183	1448.839	1434.676
8.2	1383.542	1405.971	1438.429	1433.534	1449.809	1434.779
8.25	1404.148	1409.716	1440.421	1434.927	1450.106	1434.779
8.3	1411.428	1410.138	1441.009	1435.212	1450.509	1435.002
8.35	1423.213	1412.914	1442.661	1435.826	1451.758	1439.536
8.4	1428.542	1413.496	1442.904	1436.537	1451.881	1439.536
8.45	1429.247	1416.667	1443.878	1437.070	1452.173	1451.684
8.5	1435.736	1417.407	1444.397	1438.602	1452.304	1451.852
8.55	1438.387	1417.434	1444.530	1440.088	1453.888	1456.696
8.6	1439.936	1420.455	1445.085	1440.128	1454.245	1459.011
8.65	1440.427	1421.715	1445.332	1440.354	1454.325	1459.150
8.7	1449.881	1425.065	1445.895	1440.837	1455.191	1459.936
8.75	1450.874	1425.191	1446.195	1441.248	1455.433	1460.389
8.8	1451.981	1426.350	1446.219	1441.301	1458.273	1460.623
8.85	1452.483	1427.379	1446.674	1441.460	1459.097	1461.869
8.9	1452.898	1431.664	1447.200	1441.528	1459.127	1462.584
8.95	1453.139	1432.469	1447.528	1441.545	1459.347	1466.149
9	1453.672	1432.469	1447.953	1442.131	1460.361	1467.761
9.05	1451.093	1436.650	1448.395	1442.478	1460.744	1470.489
9.1	1454.949	1436.789	1448.691	1442.497	1462.199	1471.272
9.15	1455.604	1437.162	1450.204	1443.056	1462.243	1474.621
9.2	1456.046	1437.324	1450.704	1443.209	1462.486	1474.676
9.25	1456.460	1438.134	1451.509	1443.855	1463.187	1474.779
9.3	1456.604	1440.000	1452.192	1444.334	1463.608	1475.717
9.35	1457.460	1440.316	1453.150	1444.662	1466.930	1477.445
9.4	1459.480	1440.817	1457.220	1444.757	1467.763	1479.536
9.45	1460.885	1441.319	1458.016	1444.882	1468.680	1480.421
9.5	1460.494	1441.969	1460.494	1445.240	1468.821	1480.889
9.55	1460.778	1442.011	1460.778	1445.266	1469.044	1482.506
9.6	1461.717	1442.160	1462.107	1446.029	1469.066	1483.890
9.65	1462.136	1442.160	1463.088	1446.869	1469.762	1484.341
9.7	1462.688	1442.200	1465.719	1447.355	1469.953	1484.759

Appendix Table (continued)

9.75	1462.949	1443.480	1466.696	1447.584	1473.055	1485.025
9.8	1463.604	1443.753	1467.225	1448.599	1473.649	1486.543
9.85	1464.046	1443.851	1467.225	1449.128	1473.721	1487.075
9.9	1464.460	1443.921	1467.225	1449.162	1474.615	1487.258
9.95	1464.604	1444.608	1467.225	1449.597	1475.441	1491.812
10	1465.460	1444.899	1467.225	1450.019	1477.223	1492.279

Appendix Table 2 Results of Young's Modulus from IUM Method for Group 2 Sample

Sample Thickness (mm)	Young's Modulus (MPa) Sample 2.1	Young's Modulus (MPa) Sample 2.2	Young's Modulus (MPa) Sample 2.3	Young's Modulus (MPa) Sample 2.4	Young's Modulus (MPa) Sample 2.3
0.05	1517.024	1519.565	1474.343	1512.321	1546.342
0.1	1517.911	1522.253	1477.904	1512.343	1548.128
0.15	1518.966	1524.407	1482.027	1513.031	1549.732
0.2	1519.606	1525.732	1482.222	1515.310	1550.713
0.25	1520.825	1528.342	1482.290	1518.344	1552.626
0.3	1521.734	1529.865	1485.184	1520.242	1553.841
0.35	1522.615	1531.753	1485.778	1521.775	1555.224
0.4	1524.233	1532.105	1488.151	1522.300	1556.207
0.45	1525.836	1539.897	1490.797	1536.346	1560.903
0.5	1526.875	1544.213	1492.037	1543.219	1563.578
0.55	1528.529	1544.687	1492.209	1543.588	1564.641
0.6	1530.237	1545.736	1492.475	1545.374	1566.017
0.65	1532.591	1559.574	1492.527	1571.169	1574.110
0.7	1534.622	1560.503	1493.982	1572.035	1575.587
0.75	1535.148	1560.877	1494.284	1572.175	1576.037
0.8	1538.308	1562.037	1495.568	1573.270	1578.192
0.85	1541.844	1562.527	1497.321	1573.556	1580.201
0.9	1546.132	1563.658	1497.715	1574.886	1582.905
0.95	1548.540	1565.476	1498.472	1577.115	1585.015
1	1553.352	1565.746	1498.894	1577.186	1587.550
1.05	1553.874	1567.735	1501.096	1580.731	1588.804
1.1	1554.994	1571.757	1501.136	1588.230	1591.374
1.15	1555.882	1572.315	1511.584	1589.229	1592.096
1.2	1556.449	1573.196	1514.159	1590.955	1592.819
1.25	1556.949	1574.361	1514.178	1593.091	1593.651
1.3	1557.617	1575.872	1514.285	1594.056	1594.740
1.35	1557.904	1576.596	1515.685	1595.299	1595.245
1.4	1557.966	1577.010	1516.171	1595.473	1595.483
1.45	1558.012	1577.591	1516.542	1596.219	1595.796
1.5	1558.070	1578.743	1517.121	1597.559	1596.401
1.55	1558.935	1580.812	1517.305	1600.487	1597.867
1.6	1559.838	1581.898	1518.488	1602.444	1598.860
1.65	1560.516	1583.275	1518.848	1604.913	1599.887
1.7	1561.344	1588.227	1519.672	1606.970	1602.776
1.75	1562.398	1589.479	1521.150	1608.051	1603.927
1.8	1563.250	1590.761	1522.219	1610.534	1604.994

Appendix Table 2 (continued)

1.9	1565.006	1591.852	1523.195	1612.118	1606.414
1.95	1565.868	1592.336	1523.460	1612.886	1607.086
2	1567.591	1593.919	1523.965	1615.874	1608.737
2.05	1569.615	1595.132	1525.515	1618.124	1610.353
2.1	1572.014	1598.005	1526.331	1622.396	1612.986
2.15	1573.742	1599.684	1526.720	1623.140	1614.688
2.2	1575.873	1601.949	1527.582	1626.073	1616.883
2.25	1577.877	1607.624	1527.769	1630.882	1620.719
2.3	1579.657	1613.008	1527.842	1640.865	1624.299
2.35	1582.406	1620.726	1528.994	1655.385	1629.529
2.4	1585.716	1623.566	1529.958	1660.541	1632.600
2.45	1587.871	1631.772	1538.359	1667.201	1637.778
2.5	1589.849	1637.094	1545.060	1673.100	1641.425
2.55	1595.128	1643.259	1550.323	1674.324	1647.140
2.6	1604.029	1646.932	1550.514	1678.677	1653.416
2.65	1611.015	1655.075	1554.077	1689.490	1660.971
2.7	1617.751	1659.754	1556.509	1698.121	1666.670
2.75	1625.103	1667.106	1558.257	1709.318	1674.013
2.8	1632.187	1673.242	1569.807	1710.513	1680.614
2.85	1639.046	1679.418	1580.237	1711.432	1687.122
2.9	1645.886	1686.896	1593.154	1712.650	1694.272
2.95	1653.121	1688.728	1597.355	1713.213	1698.796
3	1667.158	1693.822	1608.584	1714.111	1708.344
3.05	1670.296	1694.272	1610.662	1714.997	1710.134
3.1	1673.735	1695.405	1614.650	1715.786	1712.415
3.15	1676.961	1695.629	1616.089	1716.055	1714.136
3.2	1679.866	1696.112	1616.124	1716.891	1715.826
3.25	1683.224	1696.433	1618.045	1717.464	1717.662
3.3	1685.760	1697.629	1619.194	1719.206	1719.525
3.35	1689.497	1698.189	1619.446	1719.804	1721.669
3.4	1695.347	1698.574	1620.309	1720.418	1724.778
3.45	1700.145	1699.331	1621.423	1720.806	1727.549
3.5	1701.262	1702.205	1623.823	1725.465	1729.544
3.55	1707.956	1712.708	1641.793	1729.263	1738.133
3.6	1715.743	1718.748	1651.257	1729.401	1745.037
3.65	1722.849	1736.193	1654.204	1756.152	1757.303
3.7	1730.483	1749.857	1663.259	1771.238	1767.943
3.75	1737.741	1761.063	1668.917	1785.647	1777.165
3.8	1744.530	1776.110	1676.743	1803.824	1788.075
3.85	1753.138	1785.517	1691.387	1807.114	1797.071
3.9	1762.947	1801.760	1702.653	1824.795	1810.084

Appendix Table 2 (continued)

4.05	1783.952	1822.479	1717.021	1829.257	1815.740
4.1	1789.076	1823.523	1719.617	1830.781	1817.824
4.15	1793.072	1826.716	1720.044	1831.802	1822.895
4.2	1798.157	1827.824	1720.312	1832.239	1823.091
4.25	1803.886	1829.664	1723.425	1832.323	1825.972
4.3	1808.080	1830.211	1724.762	1833.598	1826.606
4.35	1813.038	1833.249	1728.021	1835.146	1826.908
4.4	1817.755	1837.143	1728.492	1835.949	1828.337
4.45	1822.820	1837.674	1731.685	1836.580	1830.037
4.5	1831.060	1839.043	1733.880	1836.630	1830.520
4.55	1832.453	1839.365	1735.991	1837.434	1830.919
4.6	1834.433	1839.509	1736.285	1837.929	1831.213
4.65	1835.893	1840.652	1737.016	1840.046	1831.314
4.7	1837.429	1840.915	1737.576	1840.838	1831.514
4.75	1839.172	1841.059	1737.803	1841.017	1832.190
4.8	1840.698	1841.133	1738.541	1842.715	1833.050
4.85	1842.225	1841.301	1738.623	1843.180	1833.301
4.9	1843.769	1841.508	1739.608	1843.260	1833.545
4.95	1846.537	1841.787	1740.425	1843.500	1833.590
5	1848.575	1841.917	1741.513	1844.274	1833.601
5.05	1851.658	1842.313	1741.515	1851.181	1833.997
5.1	1854.380	1842.657	1741.609	1852.684	1834.074
5.15	1858.296	1843.235	1741.729	1853.359	1834.236
5.2	1861.060	1843.511	1742.067	1854.252	1834.554
5.25	1864.150	1843.553	1743.341	1856.573	1834.691
5.3	1867.641	1843.660	1743.353	1860.058	1835.058
5.35	1870.000	1843.941	1751.902	1860.871	1835.315
5.4	1875.229	1844.555	1758.352	1861.199	1835.361
5.45	1877.543	1845.419	1762.220	1861.312	1835.526
5.5	1881.681	1845.864	1775.750	1861.624	1835.579
5.55	1883.872	1845.977	1779.557	1862.177	1835.624
5.6	1881.605	1846.372	1785.312	1862.513	1835.631
5.65	1886.373	1846.590	1807.645	1862.589	1835.983
5.7	1883.924	1847.003	1813.957	1863.056	1836.049
5.75	1886.589	1847.619	1821.043	1863.187	1836.268
5.8	1885.421	1848.127	1826.723	1863.716	1836.461
5.85	1883.850	1848.461	1837.336	1863.765	1836.648
5.9	1887.922	1848.484	1838.861	1863.855	1836.814
5.95	1886.351	1848.502	1839.270	1863.975	1836.847
6	1883.621	1848.513	1839.437	1864.069	1836.997
6.05	1883.973	1848.528	1839.589	1864.717	1837.292

Appendix Table 2 (continued)

6.15	1884.678	1848.874	1843.348	1865.915	1837.537
6.2	1885.030	1848.885	1850.639	1866.123	1837.602
6.25	1885.382	1848.923	1850.957	1866.388	1837.654
6.3	1885.734	1849.047	1854.488	1866.559	1837.696
6.35	1886.087	1849.071	1854.536	1866.602	1837.786
6.4	1886.439	1849.314	1855.607	1866.937	1837.940
6.45	1886.791	1849.345	1855.873	1868.432	1838.122
6.5	1887.498	1849.460	1856.098	1868.930	1838.140
6.55	1887.727	1849.507	1856.295	1869.143	1838.220
6.6	1887.956	1849.585	1856.623	1870.177	1838.666
6.65	1888.186	1849.831	1859.846	1870.615	1838.707
6.7	1888.415	1849.981	1860.981	1870.862	1838.883
6.75	1888.644	1850.055	1861.752	1872.688	1839.069
6.8	1888.873	1850.314	1861.899	1872.884	1839.105
6.85	1889.103	1850.335	1862.150	1872.985	1839.235
6.9	1889.332	1850.599	1862.400	1873.595	1839.262
6.95	1889.561	1850.636	1862.548	1873.709	1839.568
7	1890.020	1850.776	1862.706	1874.397	1839.619
7.05	1890.103	1850.833	1862.914	1874.645	1839.664
7.1	1890.187	1850.892	1863.130	1874.966	1839.719
7.15	1890.271	1851.267	1863.784	1875.716	1840.015
7.2	1890.355	1851.491	1864.001	1875.944	1840.086
7.25	1890.438	1851.831	1864.122	1876.197	1840.102
7.3	1890.522	1852.018	1864.178	1876.510	1840.255
7.35	1890.606	1852.098	1864.234	1876.710	1840.605
7.4	1890.690	1852.330	1864.281	1876.846	1840.738
7.45	1890.773	1852.430	1864.387	1876.899	1840.911
7.5	1890.942	1852.514	1864.585	1877.331	1841.472
7.55	1889.086	1852.623	1864.809	1877.390	1841.504
7.6	1889.271	1853.092	1865.810	1878.224	1841.596
7.65	1889.456	1853.298	1865.822	1878.668	1841.836
7.7	1889.641	1853.329	1865.833	1878.908	1841.850
7.75	1889.825	1853.624	1866.094	1879.739	1841.958
7.8	1890.010	1853.828	1866.392	1879.829	1842.127
7.85	1890.195	1854.021	1867.036	1880.189	1842.360
7.9	1890.380	1854.155	1867.069	1880.913	1842.416
7.95	1890.565	1854.283	1867.837	1880.944	1842.942
8	1890.562	1854.793	1868.004	1881.008	1843.057
8.05	1890.715	1854.882	1868.897	1881.235	1843.161
8.1	1890.867	1855.106	1869.369	1881.344	1843.161
8.15	1891.020	1855.129	1870.071	1881.829	1843.193

Appendix Table 2 (continued)

8.25	1891.325	1855.721	1870.310	1881.894	1843.715
8.3	1891.478	1855.891	1871.108	1881.949	1844.015
8.35	1891.630	1855.905	1873.451	1882.412	1844.569
8.4	1891.783	1856.251	1874.998	1882.420	1845.179
8.45	1891.935	1856.703	1881.514	1882.641	1845.499
8.5	1892.088	1856.821	1881.593	1882.692	1845.841
8.55	1892.259	1857.289	1883.934	1883.036	1848.193
8.6	1892.430	1857.460	1884.494	1883.973	1848.333
8.65	1892.565	1857.576	1885.801	1884.111	1848.527
8.7	1892.603	1857.961	1885.919	1884.619	1848.974
8.75	1892.677	1858.224	1886.276	1884.980	1849.248
8.8	1892.844	1858.303	1886.501	1885.218	1849.601
8.85	1893.097	1858.432	1886.626	1885.291	1852.039
8.9	1892.892	1859.625	1887.566	1885.310	1857.117
8.95	1893.252	1859.978	1889.085	1885.470	1859.724
9	1893.378	1860.048	1889.352	1885.710	1863.127
9.05	1893.565	1860.248	1890.701	1885.846	1867.437
9.1	1893.751	1860.365	1892.720	1885.853	1868.305
9.15	1893.938	1860.498	1892.960	1885.898	1869.527
9.2	1894.125	1860.814	1894.214	1885.911	1870.376
9.25	1894.311	1861.083	1894.498	1886.270	1871.265
9.3	1894.498	1861.706	1894.644	1886.435	1872.209
9.35	1894.684	1861.750	1894.760	1886.466	1873.137
9.4	1894.871	1861.980	1895.179	1886.573	1874.059
9.45	1895.057	1862.493	1895.945	1886.667	1874.899
9.5	1891.319	1862.992	1896.072	1886.866	1876.337
9.55	1892.797	1864.264	1896.116	1887.063	1878.073
9.6	1893.751	1867.791	1896.145	1887.453	1880.257
9.65	1892.192	1867.992	1896.214	1888.114	1881.880
9.7	1892.751	1868.700	1897.872	1888.131	1884.321
9.75	1894.292	1869.063	1897.932	1888.459	1886.080
9.8	1893.359	1869.582	1897.999	1889.152	1887.801
9.85	1891.718	1870.797	1898.367	1892.027	1889.827
9.9	1893.366	1872.105	1898.400	1892.248	1891.380
9.95	1893.176	1874.719	1900.086	1892.588	1895.742

Appendix Table 3: Results of Young's Modulus from IUM Group 3 Samples

Sample Thickness (mm)	Young's Modulus (MPa) Sample 3.1	Sample Thickness (mm)	Young's Modulus (MPa) Sample 3.2
0.075	774.073	0.025	1213.118
0.150	774.191	0.050	1214.003
0.225	774.351	0.075	1215.056
0.300	774.865	0.100	1215.694
0.375	777.277	0.125	1216.910
0.450	777.636	0.150	1217.817
0.525	777.768	0.175	1218.695
0.600	777.776	0.200	1220.309
0.675	779.514	0.225	1221.908
0.750	779.523	0.250	1222.944
0.825	779.529	0.275	1224.594
0.900	779.752	0.300	1226.298
0.975	779.830	0.325	1228.646
1.050	779.892	0.350	1230.671
1.125	780.460	0.375	1231.196
1.200	780.614	0.400	1234.348
1.275	781.030	0.425	1237.875
1.350	781.227	0.450	1242.152
1.425	781.412	0.475	1244.553
1.500	781.762	0.500	1249.353
1.575	783.505	0.525	1249.873
1.650	788.234	0.550	1250.991
1.725	789.059	0.575	1251.877
1.800	790.289	0.600	1252.442
1.875	791.370	0.625	1252.941
1.950	795.629	0.650	1253.607
2.025	796.162	0.675	1253.894
2.100	802.543	0.700	1253.955
2.175	803.831	0.725	1254.001
2.250	807.677	0.750	1254.059
2.325	818.118	0.775	1254.922
2.400	822.540	0.800	1275.823
2.475	825.276	0.825	1276.499
2.550	833.356	0.850	1277.324
2.625	836.752	0.875	1278.375
2.700	840.151	0.900	1279.226

Appendix Table 3 (continued)

2.850	849.940	0.950	1280.977
2.925	858.376	0.975	1291.836
3.000	858.617	1.000	1293.556
3.075	859.140	1.025	1295.574
3.150	859.564	1.050	1297.967
3.225	860.301	1.075	1299.691
3.300	861.248	1.100	1301.816
3.375	867.077	1.125	1303.815
3.450	879.149	1.150	1305.590
3.525	882.273	1.175	1308.332
3.600	882.947	1.200	1311.634
3.675	883.004	1.225	1313.784
3.750	883.464	1.250	1325.756
3.825	883.649	1.275	1331.021
3.900	883.990	1.300	1339.900
3.975	884.122	1.325	1346.867
4.050	884.650	1.350	1353.586
4.125	891.897	1.375	1360.919
4.200	901.776	1.400	1367.985
4.275	905.594	1.425	1374.826
4.350	918.019	1.450	1381.649
4.425	922.754	1.475	1388.865
4.500	931.126	1.500	1412.866
4.575	933.654	1.525	1415.996
4.650	940.610	1.550	1419.426
4.725	941.445	1.575	1422.643
4.800	944.701	1.600	1425.541
4.875	956.145	1.625	1428.891
4.950	957.733	1.650	1431.420
5.025	958.553	1.675	1435.148
5.100	959.744	1.700	1440.982
5.175	963.623	1.725	1445.768
5.250	964.268	1.750	1456.882
5.325	965.226	1.775	1463.559
5.400	967.434	1.800	1471.326
5.475	968.058	1.825	1478.413
5.550	970.048	1.850	1486.028
5.625	972.002	1.875	1493.268
5.700	972.249	1.900	1500.039
5.775	975.835	1.925	1508.625
5.850	976.039	1.950	1518.408

Appendix Table 3 (continued)

6.000	978.307	2.000	1534.247
6.075	979.663	2.025	1539.359
6.150	980.132	2.050	1544.471
6.225	984.195	2.075	1548.456
6.300	986.420	2.100	1553.528
6.375	995.853	2.125	1559.242
6.450	999.153	2.150	1573.425
6.525	999.353	2.175	1578.371
6.600	1001.275	2.200	1583.076
6.675	1001.621	2.225	1588.128
6.750	1003.678	2.250	1596.347
6.825	1003.693	2.275	1597.735
6.900	1011.433	2.300	1599.710
6.975	1012.418	2.325	1601.021
7.050	1018.046	2.350	1609.900
7.125	1018.955	2.375	1616.867
7.200	1020.459	2.400	1623.586
7.275	1022.757	2.425	1630.919
7.350	1026.427	2.450	1637.985
7.425	1029.209	2.475	1644.826
7.500	1029.934	2.500	1651.649
7.575	1030.533	2.525	1658.865
7.650	1030.781	2.550	1682.866
7.725	1031.602	2.575	1685.996
7.800	1031.634	2.600	1689.426
7.875	1031.644	2.625	1692.643
7.950	1033.397	2.650	1695.541
8.025	1038.216	2.675	1695.739
8.100	1039.652	2.700	1695.768
8.175	1040.466	2.725	1696.882
8.250	1041.343	2.750	1698.891
8.325	1042.267	2.775	1701.420
8.400	1044.165	2.800	1703.559
8.475	1047.509	2.825	1703.559
8.550	1050.569	2.850	1705.148
8.625	1051.408	2.875	1710.982
8.700	1052.343	2.900	1711.326
8.775	1055.233	2.925	1711.326
8.850	1057.154	2.950	1715.768
8.925	1057.744	2.975	1718.413
9.000	1062.068	3.000	1718.413

Appendix Table 3 (continued)

9.150	1064.284	3.050	1726.028
9.225	1066.736	3.075	1726.882
9.300	1067.155	3.100	1733.268
9.375	1069.004	3.125	1733.268
9.450	1071.731	3.150	1733.559
9.525	1074.784	3.175	1740.039
9.600	1075.241	3.200	1740.039
9.675	1076.964	3.225	1741.326
9.750	1076.981	3.250	1748.413
9.825	1078.131	3.275	1748.625
9.900	1078.977	3.300	1748.625
9.975	1080.171	3.325	1756.028
10.050	1084.821	3.350	1758.408
10.125	1091.480	3.375	1758.408
10.200	1101.955	3.400	1763.268
10.275	1123.613	3.425	1765.065
10.350	1124.335	3.450	1765.065
10.425	1143.612	3.475	1770.039
10.500	1148.072	3.500	1774.247
10.575	1151.386	3.525	1774.247
10.650	1157.352	3.550	1778.625
10.725	1158.942	3.575	1779.359
10.800	1160.164	3.600	1779.359
10.875	1160.958	3.625	1784.471
10.950	1161.411	3.650	1784.471
11.025	1161.560	3.675	1788.408
11.100	1161.736	3.700	1788.456
11.175	1162.628	3.725	1788.456
11.250	1163.793	3.750	1793.528
11.325	1164.318	3.775	1795.065
11.400	1165.452	3.800	1799.242
11.475	1165.592	3.825	1803.425
11.550	1166.151	3.850	1804.247
11.625	1167.042	3.875	1808.371
11.700	1167.650	3.900	1809.359
11.775	1168.410	3.925	1813.076
11.850	1168.823	3.950	1814.471
11.925	1168.905	3.975	1818.128
12.000	1169.198	4.000	1818.456
12.075	1170.703	4.025	1823.528
12.150	1171.314	4.050	1826.347

Appendix Table 3 (continued)

12.300	1172.218	4.100	1829.242
12.375	1173.128	4.125	1829.710
12.450	1179.289	4.150	1831.167
12.525	1181.272	4.175	1832.699
12.600	1184.621	4.200	1834.437
12.675	1184.676	4.225	1835.959
12.750	1184.779	4.250	1837.482
12.825	1185.002	4.275	1839.022
12.900	1189.536	4.300	1841.783
12.975	1201.684	4.325	1843.425
13.050	1201.852	4.350	1843.816
13.125	1206.696	4.375	1846.891
13.200	1209.011	4.400	1848.371
13.275	1209.150	4.425	1849.606
13.350	1209.936	4.450	1853.076
13.425	1221.272	4.475	1853.512
13.500	1224.621	4.500	1856.269
13.575	1224.676	4.525	1858.128
13.650	1224.779	4.550	1859.350
13.725	1228.239	4.575	1862.833
13.800	1228.467	4.600	1865.185
13.875	1229.386	4.625	1870.401
13.950	1229.536	4.650	1872.709
14.025	1229.979	4.675	1876.761
14.100	1230.077	4.700	1876.837
14.175	1230.114	4.725	1879.000
14.250	1230.421	4.750	1879.022
14.325	1230.748	4.775	1879.074
14.400	1230.886	4.800	1880.567
14.475	1230.922	4.825	1881.495
14.550	1231.641	4.850	1881.516
14.625	1231.733	4.875	1881.732
14.700	1231.809	4.900	1883.062
14.775	1232.242	4.925	1886.450
14.850	1232.621	4.950	1887.321

Appendix Table 4 Table of DoC and Corresponding Young's Modulus From different Measurement Locations

Sample No.	DoC			Modulus MPa		
	Center	left	right	center	left	right
1.1	0.447	0.421	0.435	1404.259	1320.996	1364.701
1.2	0.464	0.434	0.433	1423.091	1332.132	1359.541
1.3	0.470	0.445	0.452	1447.288	1396.317	1419.354
1.4	0.485	0.468	0.472	1461.956	1469.793	1480.432
1.5	0.492	0.487	0.482	1477.349	1528.343	1512.338
1.6	0.504	0.511	0.503	1491.796	1602.999	1577.521
2.1	0.787	0.782	0.677	1804.276	1574.044	1497.153
2.2	0.803	0.787	0.683	1811.536	1526.785	1516.693
2.3	0.817	0.808	0.695	1827.865	1619.893	1552.315
2.4	0.822	0.730	0.677	1839.620	1663.134	1496.402
2.5	0.824	0.804	0.720	1850.144	1648.399	1631.567
3.1	0.440	0.404	0.413	1380.143	1269.369	1296.778
3.2	0.809	0.766	0.739	1811.716	2183.826	1690.155
4.1 R1	0.263	0.254	0.246	825.313	796.858	772.513
4.1 R2	0.265	0.238	0.244	832.515	747.739	765.454
4.2 R1	0.385	0.382	0.382	1208.601	1198.662	1199.828
4.2 R2	0.391	0.393	0.388	1214.412	1231.791	1217.111

Appendix Table 5: Evaluated Damping ratio for each Sample, from IUM Measurements and Nanoindentation Measurements

Sample No.	Damping Ratio (IUM Measurements)	Damping Ratio (Nanoindentation Masurements)
1.1	0.075	0.057
1.2	0.075	0.058
1.3	0.076	0.062
1.4	0.076	0.064
1.5	0.075	0.055
1.6	0.075	0.059
2.1	0.053	0.041
2.2	0.053	0.036
2.3	0.053	0.036
2.4	0.052	0.031
2.5	0.051	0.034
3.1	0.083	0.066
3.2	0.045	0.020
4.1 R1	0.038	0.018
4.1 R2	0.038	0.022
4.2 R1	0.048	0.021
4.2 R2	0.047	0.025

Appendix Table 6: Calculation Results of Loss Factor From Section 3.3

Sample No.	Loss Factor from Method 1 (IUM)	Loss Factor from Method 2 (Nanoindentation)	Difference in Loss Factor from the two methods
1.1	0.153	0.148	3.4%
1.2	0.152	0.146	3.6%
1.3	0.154	0.149	3.6%
1.4	0.154	0.150	2.7%
1.5	0.152	0.153	1.3%
1.6	0.154	0.165	6.9%
2.1	0.103	0.108	5.0%
2.2	0.103	0.098	5.8%
2.3	0.104	0.109	4.8%
2.4	0.104	0.112	7.2%
2.5	0.103	0.097	5.9%
3.1	0.167	0.176	5.3%
3.2	0.088	0.083	6.9%
4.1 R1	0.076	0.081	6.2%
4.1 R2	0.076	0.077	1.0%
4.2 R1	0.094	0.100	6.0%
4.2 R2	0.091	0.088	3.0%

Appendix Table 7: Calculated Young's Modulus for Set 2 Samples with IUM and FTIR two Ex-situ Methods and Correspoding Error %

Experimental Group	Sample No	Set 2 Sample 10 Layers				
		In-situ IUM Measurements (MPa)	Ex-situ FTIR based Measurements (MPa)	IUM Error% to FTIR	Ex-situ Nanoindentation based Measurements (MPa)	IUM Error% to indentation
Group 1: Varying stage speed	1.1	767.111	828.560	7.416%	813.505	5.703%
	1.2	791.372	849.864	6.882%	832.306	4.918%
	1.3	827.004	879.959	6.018%	866.944	4.607%
	1.4	842.801	894.824	5.814%	883.718	4.630%
	1.5	862.183	913.402	5.608%	904.866	4.717%
	1.6	877.048	917.359	4.394%	913.666	4.008%
Group 2: Varying layer curing time	2.1	1071.019	1152.161	7.043%	1127.121	4.977%
	2.2	1094.321	1168.422	6.342%	1145.164	4.440%
	2.3	1153.090	1234.475	6.593%	1207.813	4.531%
	2.4	1194.044	1278.407	6.599%	1252.283	4.651%
	2.5	1232.399	1316.256	6.371%	1290.034	4.468%
Group 3: Varying layer thickness	3.1	775.484	857.945	9.611%	816.035	4.969%
	3.2	1245.314	1331.071	6.443%	1307.457	4.753%
Group 4*: Varying light Intensity	4.1 R1	337.118	359.130	6.129%	343.768	1.934%
	4.1 R2	333.768	351.526	5.052%	341.111	2.152%
	4.2 R1	644.778	687.404	6.201%	667.997	3.476%
	4.2 R2	671.273	720.403	6.820%	698.682	3.923%

Appendix Table 8: Calculated Intermediate Young's Modulus for Set 1 Sample with IUM Method and Corrsesponding Error%

Experimental Group	Sample No.	Set 1 Intermediate Part (first 10-layers)		
		In-situ (IUM) Measurements (MPa)	IUM Error% 9Used Set 2 FTIR	IUM Error % (used Set 2 Nanoindentation
Group 1: Varying stage speed	1.1	794.111	4.158%	2.384%
	1.2	812.372	4.412%	2.395%
	1.3	831.545	5.502%	4.083%
	1.4	853.089	4.664%	3.466%
	1.5	872.545	4.473%	3.572%
	1.6	882.176	3.835%	3.446%
Group 2: Varying layer curing time	2.1	1102.102	4.345%	2.220%
	2.2	1119.346	4.200%	2.254%
	2.3	1176.216	4.719%	2.616%
	2.4	1207.399	5.554%	3.584%
	2.5	1263.376	4.017%	2.067%
Group 3: Varying layer thickness	3.1	1273.407	4.332%	2.604%
	3.2	764.484	10.894%	6.317%
Group 4*: Varying light Intensity	4.1 R1	348.831	2.868%	1.473%
	4.1 R2	353.281	0.499%	3.568%
	4.2 R1	651.158	5.273%	2.521%
	4.2 R2	658.279	8.624%	5.783%

Appendix B Photos Cured sample and Sample Surface Under Microscope

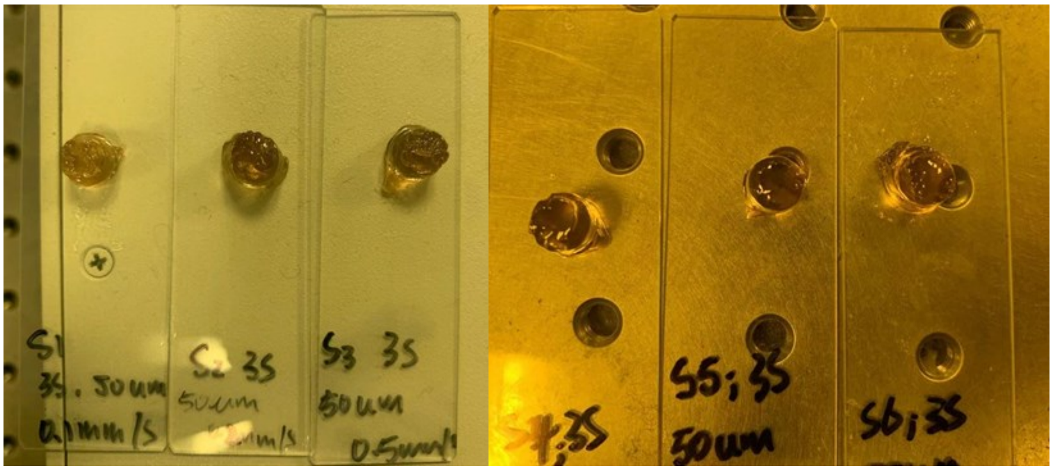

Appendix Figure 1 Photo for sample 1-6

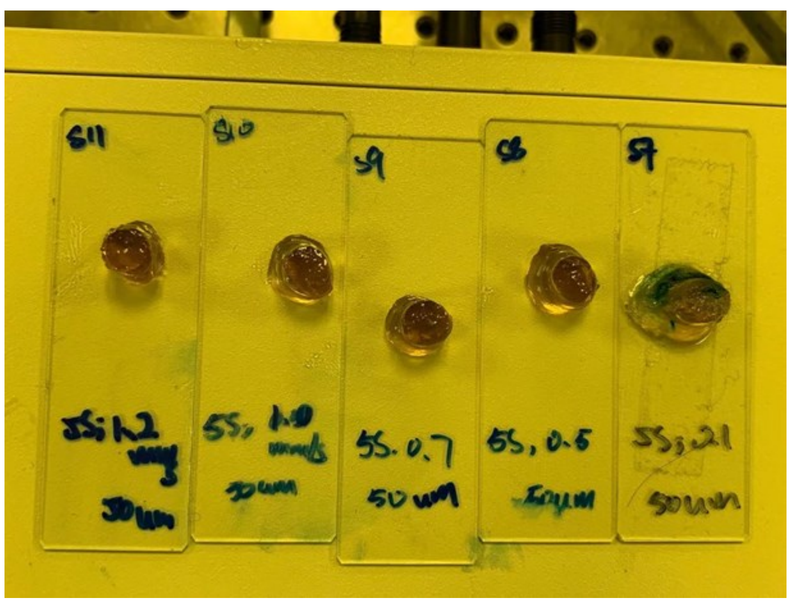

Appendix Figure 2 Photo for sample 7-11

Appendix Figure 3 Photo for sample 12-17

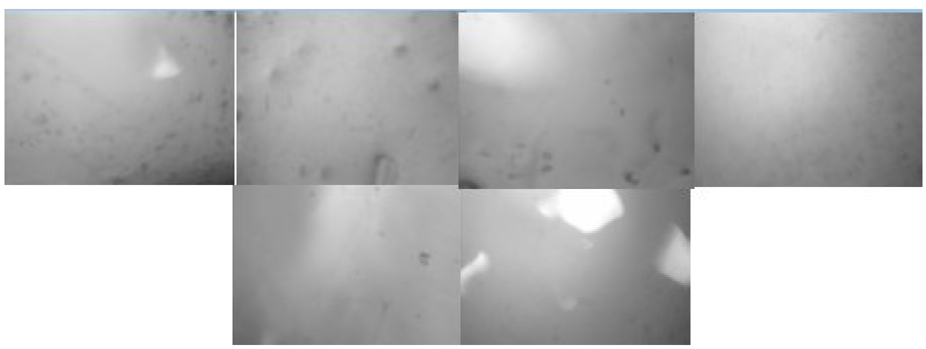

Appendix Figure 4 Photo for sample 1,3,5,7,11,14,17 surface under microscope

Appendix C Molecular Structure for Monomers

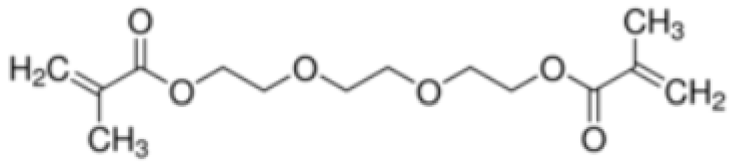

Appendix Figure 5 Chemical Bonds For triethylene glycol dimethacrylate

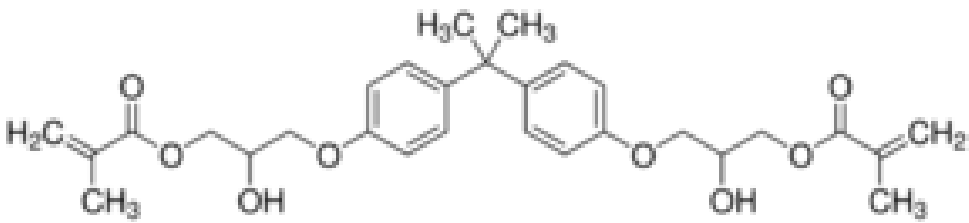

Appendix Figure 6 Chemical Bonds for bisphenol A glycidyl methacrylate

Bibliography

Andrejewska, E. (2001). Photopolymerization kinetics of multifunctional monomers. . *Progress in Polymer Science 26*, 605-665.

Bennett, J. (2017). Measuring UV Curing Parameters of Commercial Photopolymerization used In Additive Manufacturing. *Additive Manufacturing 18*, 203-212.

Bruker. (2014). *TI 950 Triboindenter User Manual.* Hysitron Incorporated .

C.H.Wong, Q. &. (2017). Additive Manufacturing Process Monitoring Controlled by Non-Destrcutive Testing Technique: Challenges and In Process Monitoring. *Virtual and Physcial Prototyping*, Volume 14 Issue 3.

Charlesby, A. (1992). Elastic modulus formilae for a crosslined network. *Journal of Radiation Applications and Instrumentation Part C, Radication Physics & Chemistry 40*, 117-120.

Chen, M., Zhong, M. & Jognson, J. (2016). A. Light-Controlled Radical Polymerization Mechnisms, Methods and Applications. *Chem Reviews 116*, 10167-10211.

D.C, A. M. (2006). A new Kinetic Model for the Photopolymerization Shrinkage-Starin of dental composite and resin monomers. *Dent Mater 22*, 785-791.

Franck, A. (2018). *Viscoelasticitu and Dynamic Mechanical Testing.* Germany: TA Instruments.

Gates, T. (2007). Characterization of Viscoelastic Properties of Polymeric Material Through Nanoindentation . *Experimental Materials* .

Gibson, I, Rosen and Stuker B. (2014). *Additive Manufacturing Technologies: 3D Printing, Rapid Prototyping and Dircet Digital Manufactuering 2nd Edition.* New York: Springer Verlag.

Higgins, C. I. (2020). Digital Light Processing in a Hybrid Atomic Force Microscope: In situ, nanoscale Characterzation of the Printing Process. *Additive Manufacturing 38*.

Hornbeck, L. (1996). Digital Light Processing and MEMS: an overview. *Summer Topical Meeting. Advanced Applications of Lasers in Materials and Processing,* (pp. 7-8). Keystone CO USA: IEEE.

Krautkramer, J., Krautkramer, H. (2013). *Ultrasonic Testing of Materials.* Berlin: Springer Science and Bussiness Media.

Kuar, M. &. (2002). Photopolymerization: A Review. *Journal of Macromolecular Science, Part C: Polymer Reviews 42*, 481-512.

Li, Q. (2016). Chaacterization of material fabricated by Additive manufacturing method using Line focused Ultrasonic Transducer. *IMECE.* Phoenix.

Liu, W. (2008). *Experimental and Anlytical Estimationg of Damping in Polymers.* Kansas: University of Kansas.

Macoice, P. (2010). *Viscoelatsic Damping 101.* Rousb Industries Inc.

Mao Chen, Mingjiang Zhong. (2016). Light Controlled Radical Polymerization: Mechanisms Methods and Applications. *Chemical Reviews*, 10167-10211.

Marten, F. a. (1982). High Conversion Diffusion-Controlled Polymerization of Styrene I. *Journal of Applied Polymer Science Vol 27*, 490-505.

Marting P de Beer, Harrt L, van der Laan. (2019). Rapid, continuous Addtive Manufacturing by Volumeteric Polymerization Inhibition Patterning. *Science Advance*, Vol.5 No. 1.

Miller, D. V. (1979). Calculation of Molecular Parameter of Stepwise Polyfunctional Polymerization. *Polymer Engineering and Science Vol 19*, 272-283.

Odegar, G.M., Herrings, H.M. (2005). Characterization of Viscoelatic Properties of Polymeric Material Through Nanoindentation. *Society for Experimental Mechanics*, 130-137.

Odian, G. (2004). *Principles of polymerization. Fourth Edition edn.* John Wiley & Sons,.

Pritz, T. (2001). Loss factor peaks of Visctoelactis Materials. *Sound and Vibration*, 265-280.

Takezawa, A. (2015). Porous compositie with negative thermal expansion Obtained by Photopolymer Additive Manufacturing. *APL Materials 3.7*.

Tang, Y. (2005). *Stereolithography Cure Process Modeling.* Georgia Institude od Technology.

Venkata Karthik Nadipalli, L. Y. (2018). In-sity interfactial quality assesment of Ultrasonic Additive Manufacturin Component using Ultrasonic NDE. *NDT and E International*, 117-130.

Wang, J., Zhao, C., Zhang, Y., Jariwala, A., & Rosen, D. (2017). Process Modeling And In-situ Monitoring Of Photopolymerization For Exposure Controlled Projection Lithography. *An Additive Manufacturing Conference.* Knoxville, TN.

Wang, S. (2020). Implementation of an Elastoplastic constitutive Model for 3D printed material Favricated by Stereolithography. *Additive Manufacturing 33*.

Wohlers, T. C. (2016). *3D printing and additive manufacturing state of the industry annual worldwide progress report.* Wholers Associates, Inc.

Wu, J., Zhao, Z., Hamel, C.M., Mu, X. (2018). Evolution of material properties during free radical photopolymerization. *Jounrnal of the Mechanics and Physics of Solids 112*, 25-49.

Xiang, Y. S. (2020). Mechanical characterization and consitutive modeling of viscoelastive hyperelasticity of photocuring polymers . *Additive Manufacturing*, 101511.

Xu, X.,Vallabh, C.K.P., Cleland, Z. J., Cetinkaya, C. (2017). Phonoic Crystal Artifacts for Real Time In Situ Quality Minitoring in AdditiveManufacturing. *Journal of Manufacturing Science and Enginneirng*, Vol 139.

Y. Zhang, R. A. (2013). A Rapid Method of Measuring the glass transition Temperature using a Novel Dynamic Mechanical Analysis Method. *The Journal of Adhesion*, 785-806.

Yablon, G. D. (2015). Measureing the Loss Tangent of Polymer Materials with Atomic Force Microsopy Base Methods. *Measurement Science and Technology*, 25-34.

Yasser Zare, K. Y. (2019). Prediction of Loss factor for Pokymer Nanocomposites as a fuction of yield stress, relaxation time and the width of Transition Region Between Nwetonian and Power-Law Behvaior. *Journal of Mechanial Behavior of Biomdical Materials*, 136-143.

Zhao, X., Rosen, D,W. (2017). Real-time interferometric monitoring and measuring of photopolymerization based stereolithopgraphic additive manufacturing process: snesoe model and algorithm. *Measurement Science and Technology*, Volume 28, Issue 1.

Zhao, X., Rosen, D.W. (2018). An Implementation of Real-time Feedback Control of Cured Part Height in Exposure Controlled Projection Lithography with IN-Situ Interferometric Measurement Feedback. *Additive Manufacturing 23*, 253-263.